WP3

Monitoring network improvement for coastal flooding and extreme weather risk management

Activity 3.4
Coastal wind profiler procurement and installation

D3.4.1
A report on verification of wind forecast in Dubrovnik area before and after installation of wind profiler

European Regional Development Fund

www.italy-croatia.eu/acronym

PROJECT AND ACTIVITY DETAILS

Project Acronym	AdriaMORE
Project title	Adriatic DSS exploitation for MOnitoring and Risk management of coastal Extreme weather and flooding
Funding Line	Priority Axis 2, Specific Objective 2.2
Project Partners	LP Abruzzo Region (Italy) P1 Dubrovnik and Neretva Region (Croatia) P2 Meteorological and hydrological service (Croatia) P3 National Research Council (Italy)
Starting date	January 1, 2018
Work Package	WP4: Monitoring network improvement for coastal flooding and extreme weather risk management
Activity number	3.4
Activity Title	Coastal wind profiler procurement and installation
Deliverable number	3.4.1
Deliverable Title	A report on verification of wind forecast in Dubrovnik area before and after installation of wind profiler
Authors	Kreso Pandzic (DHMZ), Frank Marzano (CETEMPS), Davor Tomsic (DHMZ)
Data of issue	30 June 2019
Total Number of pages	30
Distribution list	Italy-Croatia CBC Programme, AdriaMORE partners

This document has been produced with the contribution of the EU co-financing and the Interreg Italy-Croatia CBC Programme. The content reflects the author's views; the Programme authorities are not liable for any use that may be made of the information contained therein.

Deliverable 3.4.1

A Report on Verification of Wind Forecast in Dubrovnik Area before and after Installation of Wind Profiler

Krešo Pandžić (DHMZ), Frank Marzano (CETEMPS), Davor Tomšić (DHMZ)

1 Introduction

Under “Activity 3.4 Coastal wind profiler procurement and installation” a procurement and installation of wind profiler at Dubrovnik weather station (Figure 1) has been planned for nearly continuously updated vertical profiles of wind because of lack of upper air wind observation in neighbour countries easterly of the Sothern Croatia (Figure 2). This is radar-like instruments that point upward, and the clear-air echo returned by various layers can be processed to yield information about those layers. A profile of such velocities can be used to determine the vertical shear, which is also of importance to aviation, especially during take off and landing. Its data will be also used in the meteorological forecast model for coastal monitoring in the assimilation procedure, its data will be useful in order to provide the wind field.

It is complementary equipment to existing instruments for surface observation of wind and other meteorological parameters deployed at Dubrovnik weather station. It will measure wind speed and direction up to 3 km above the ground at least with high time resolution e.g. each 15 minutes. These data will fill the gap for upper-air wind data in the region with very complex terrain surrounding Adriatic sea.

The following steps are planned: site preparation at Dubrovnik weather station, wind profiler procurement, installation and commissioning. A comparison of verification of wind forecast in the area by NWP model without and by wind profiler data will be done.

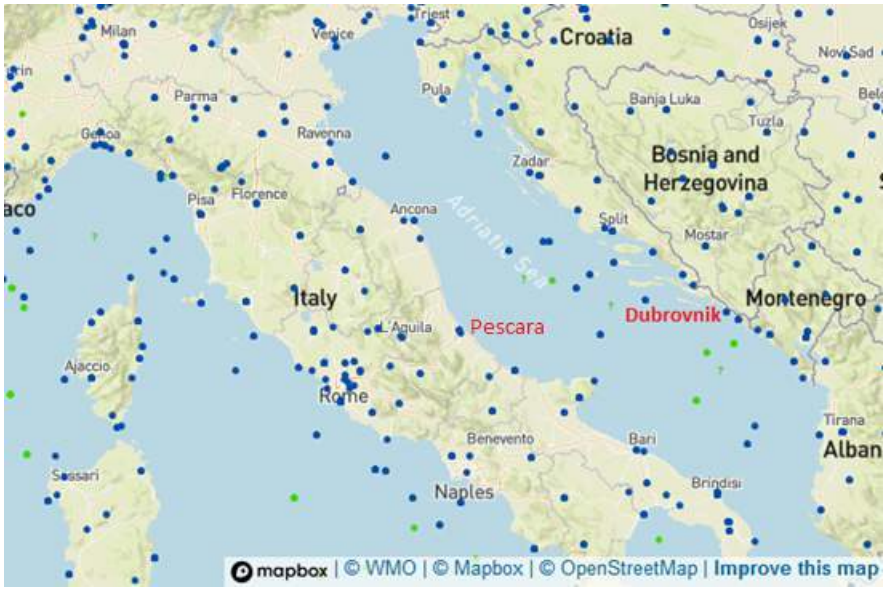

Figure 1 Distribution of surface weather stations in Adriatic region according to WMO OSCAR[1] weather station meta data base (source: https://oscar.wmo.int/) .

[1]The Observation Systems Capability Analysis and Review Tool

Figure 2 Distribution of radiosonde upper air stations (source: https://www.wmo.int).

Extreme weather conditions are rather frequent in Adriatic region. Thus, extreme winds Bora and Sirocco have a speed up to 100 kilometres per hour. Bora blows perpendicularly on the Eastern Adriatic coast and Scirocco blows paralel to the eastern Adriatic coast (see e.g. Pandžić and Likso, 2005). Synoptic conditions during both Bora and Scirocco winds are represented in Figure 3 and Figure 4, respectively. In Figure 3, a centre of high in air pressure, reduced on sea level, is dominant over European land and low pressure centre is in central Mediterranean area. A relatively cold air is in the hinterland of the Eastern Adriatic. In the case of Sirocco wind over Adriatic a synoptic scale low of sea level pressure centre is northerly from Adriatic and an advection of relatively warm air prevails over Adriatic. Bora is relatively dry and Sirocco relatively warm wind, both of them are more frequent during cold part of a year than during warmer part of the year, the Bora is more frequent in the Northern Adriatic while Sirocco is more frequent in the Southern Adriatic. In addition to the cited, the Sirocco makes bigger waves on the open sea than Bora, but Bora is more gusty than Sirocco.

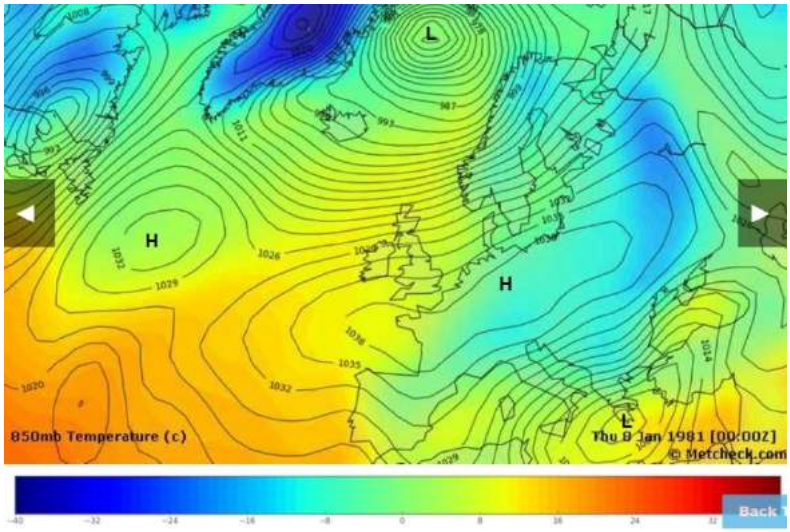

Figure 3 Distribution of sea level air pressure (hPa) and air temperature on 850 hPa constant pressure surface, on a height about 1500 m above sea level, for 8 January 1981 at 00 UTC, during Bora wind on Eastern Coast of Adriatic Sea.
(source: http://www.metcheck.com/WEATHER/gfs_reanalysis_1871_now.asp#)

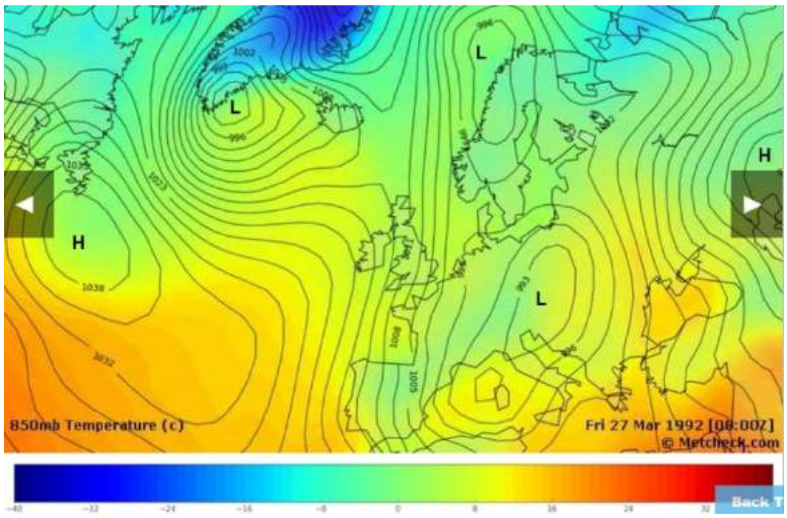

Figure 4 Distribution of sea level air pressure (hPa) and air temperature on 850 hPa constant pressure surface, on a height about 1500 m above sea level, for 27 March 1992 at 00 UTC, during Scirocco wind on Eastern Coast of Adriatic Sea.
(source: http://www.metcheck.com/WEATHER/gfs_reanalysis_1871_now.asp#)

Thunderstorms, followed by heavy precipitation and strong wind, are recognised as severe weather events on Adriatic including flash flooding recently rather frequent in South-Eastern part of Adriatic area. Ivančan Picek et al.(2007) considered possible forcing mechanisms of a heavy precipitation event in the southeastern Adriatic area. The mechanisms responsible for the formation of convection were analysed using synoptic and satellite observation data and numerical experiments were performed with the WRF (Weather Research and Forecast) model, which was set up at the convection-permitting resolution in the innermost domain. It is clear from Figure 5 that observed 24-precipitation amounts have a better agreement with WRF numerical model simulated precipitation amounts with orography than in the case when WRF simulation has been done without orohraphy.

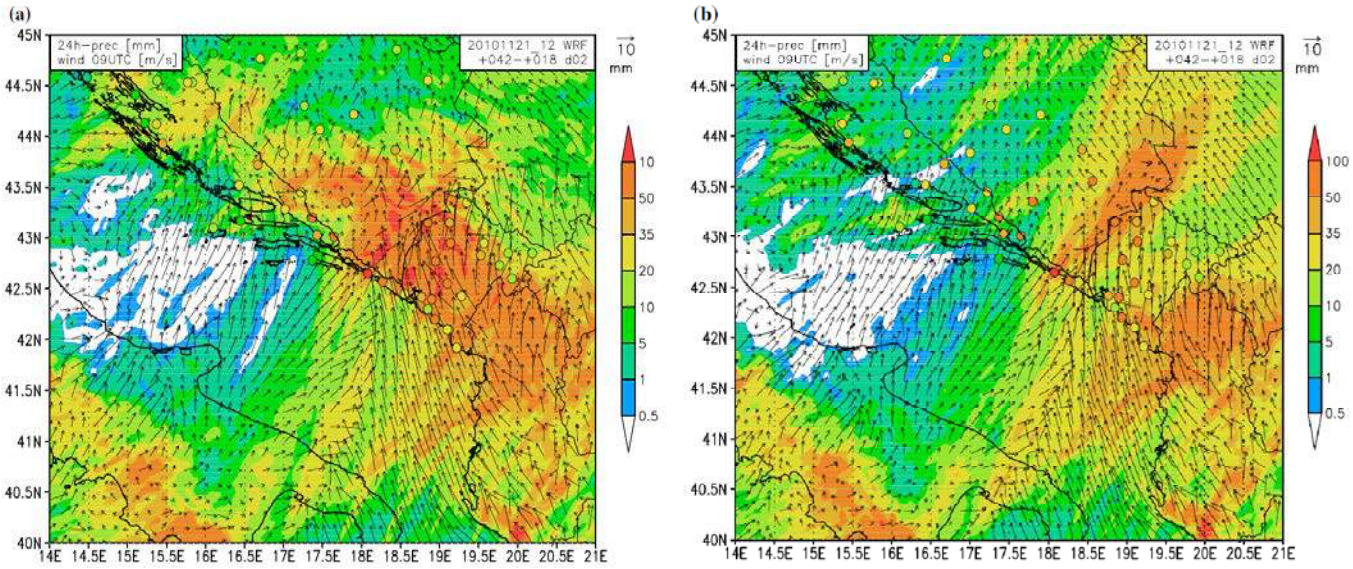

Figure 5 24-h observed (circle) and modelled precipitation (mm, shaded as in legend) from 22 to 23 November 2010 at 06 UTC and 10-m wind vectors at 09 UTC 22 November 2010: a) simulation with orography and b) simulation without orography. The area corresponds to the inner model domain (2-km grid spacing). (source: Ivančan Picek et al., 2014)

Wind profiler procurement, installation and commissioning has successfully been finished on 28 May 2019 by Meteorological and Hydrological Service (DHMZ) by a support of Dubrovnik Neretva County, both from Croatia. Big efforts has been done by CETEMPS[2] University of L'Aquila in *Italy* (also co-author of this report) for running WRF numerical atmospheric model and creation of model image outputs for two pilot case studies from June 2019. Pilot case studies have been done for 1-st and 28-th June 2019, the coldest and the warmest days in that month.

2 Statistical interpolation (objective analysis) of wind field

2.1 Representation of wind in a coordinate system

The horizontal wind vector, $\mathbf{v_H}$, is represented by the bold black line in Figure 6; **i** and **j** represent unit vectors towards East and North, respectively. Equations for converting horizontal wind vector information between the different notation conventions are given at the end of this section.

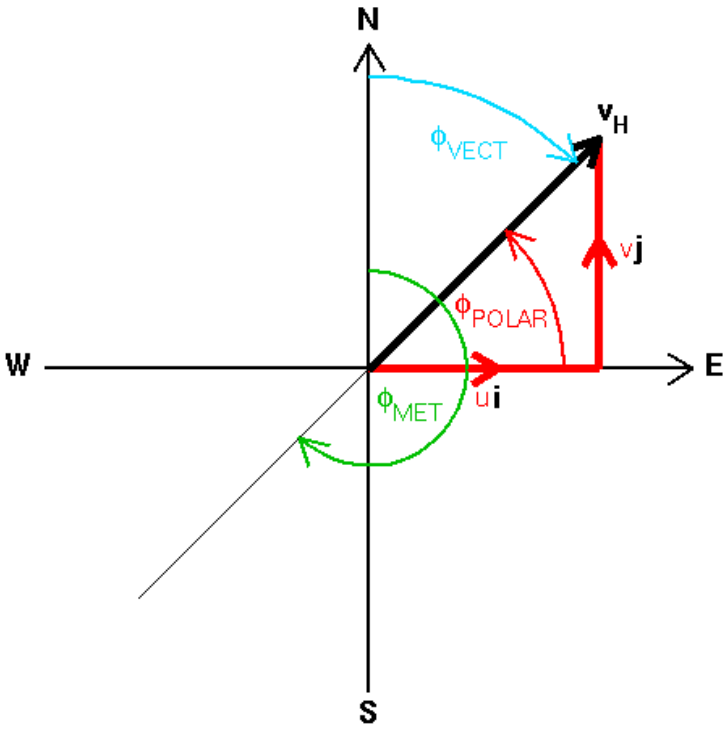

Figure 6 Representation of horizontal wind vector in a coordinate system.
(source: http://tornado.sfsu.edu/geosciences/classes/m430/Wind/WindDirection.html)

The wind vector can be expressed either in terms of orthogonal velocity components, where:

- *u* is the zonal wind component, i.e. the component of the horizontal wind in direction west-east.
- *v* is the meridional wind component, i.e. the component of the horizontal wind in direction south-north.
- *w* is vertical component of wind, which is typically positive for an upward motion

or

[2] Center of Excellence in Tele-sensing of Environment and Model Prediction of Severe Events

- as a wind speed, i.e. $|\mathbf{v_H}|$, and direction.

Particular care should be taken when dealing with the direction since two opposite conventions are commonly used:

> φ_{VECT} is the wind vector azimuth, i.e. the direction towards which the wind is blowing. It increases clockwise from North when viewed from above. Terms such as northward, eastward etc. imply wind vector azimuths.
>
> φ_{MET} is the meteorological wind direction, i.e. the direction from which the wind is blowing. It also increases clockwise from North when viewed from above. Terms such as northerly, easterly etc. imply meteorological wind directions.

These directions are typically expressed in units of degrees, φ(deg), but can either be in the interval -180° to +180° or 0° to 360°. The wind vector azimuth and meteorological convention direction are related by:

$$\phi_{MET}(deg) = \phi_{VECT}(deg) + 180$$

subtracting 360° where appropriate in order to keep the values within the desired range. Note that when writing a computer program to convert between speed/direction and orthogonal component conventions, the use of trigonometric functions assumes that angles are expressed in units of radians, φ(rad), rather than degrees (pocket calculators can typically perform trigonometric functions on angles expressed in either units). Directions are converted from units of degrees to radians through the relationship:

$$\phi(rad) = \frac{\pi}{180} \times \phi(deg)$$

Moreover, the familiar expressions relating the x component of a vector to the cosine of its angle and the y component to its sine imply use of:

> φ_{POLAR} which is the wind vector polar angle in two-dimensions. It increases anticlockwise form positive x-axis, i.e. from direction west-east; this in the opposite sense to the wind vector azimuth and the meteorological wind direction, and from a different origin.

When converting back from orthogonal components to speed and direction, the **atan2(y,x)** function in FORTRAN should be used in order to avoid ambiguity in the returned value of the wind vector polar angle. The expressions below can be used to convert horizontal wind vector information directly between the orthogonal component and speed/direction conventions without the need for first converting directions between wind the vector polar angle and the wind vector azimuth or meteorological wind direction.

Wind Vector Azimuth	Meteorological Wind Direction
$u = \lvert\boldsymbol{v_H}\rvert \times \sin\left[\frac{\pi}{180} \times \phi_{VECT}(deg)\right]$	$u = -\lvert\boldsymbol{v_H}\rvert \times \sin\left[\frac{\pi}{180} \times \phi_{MET}(deg)\right]$
$v = \lvert\boldsymbol{v_H}\rvert \times \cos\left[\frac{\pi}{180} \times \phi_{VECT}(deg)\right]$	$v = -\lvert\boldsymbol{v_H}\rvert \times \cos\left[\frac{\pi}{180} \times \phi_{MET}(deg)\right]$

$$\phi_{VECT}(deg) = \frac{180}{\pi} \times \text{atan2}(u, v) \qquad \phi_{MET}(deg) = \frac{180}{\pi} \times \text{atan2}(-u, -v)$$

$$|\boldsymbol{v_H}| = \sqrt{u^2 + v^2}$$

2.2 Autocorrelation Wind Component Functions

Empirical autocorrelation functions are basic tool for spatial statistical interpolation of meteoro - logical variables on grid points using background and observation data (Daley, 1991). More available observation data means more precise interpolated (estimated) values of meteorological variables on grid point method. Goal of this section is to show how important influence is upper air wind observation on objective analysis of wind components in upper atmosphere. Then results can also be applied on estimation of importance of wind observation by wind profiler recently installed at Dubrovnik weather station inside AdriaMORE Project..

Autocorrelation of *u* and *v* wind component functions can be simplified introducing longitudinal and transverse velocity components shown in Figure 7. At two spatial locations 1 and 2, define *l* to be the wind component along the line connecting the two points and *t* to be wind component in the direction perpendicular to *l*, positive to the left. Thus, the eastward and northward wind components (u_1, v_1) and (u_2, v_2) are replaced by (l_1, t_1) and (l_2, t_2) as shown in Figure 7. *l* and *t* are related to *u* and *v* by:

$$\begin{aligned} l &= u\cos\phi + v\sin\phi \\ t &= -u\sin\phi + v\cos\phi \end{aligned} \qquad (2.2.1)$$

where ϕ is angle between the *x* (east-west) axis and *l* measured positive counter clockwise as in planar coordinate system.

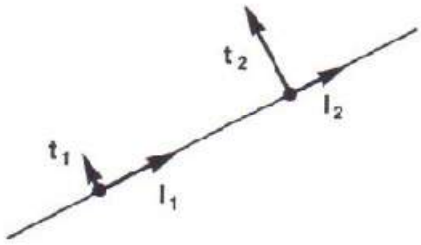

Figure 7 Longitudinal and transverse wind velocity components (after Daley, 1991).

Using above transformation the equations for calculation of longitudinal and transverse wind component autocorrelations can be derived:

$$\rho_{ll}(r) = -\left[L_\psi^2 \left(1 - \nu^2\right) \frac{1}{r}\frac{d}{dr}\rho_{\psi\psi} + L_\chi^2 \nu^2 \frac{1}{r}\frac{d^2}{dr^2}\rho_{\chi\chi} \right] \qquad (2.2.2)$$

$$\rho_{tt}(r) = -\left[L_\psi^2 \left(1 - \nu^2\right) \frac{1}{r}\frac{d^2}{dr^2}\rho_{\psi\psi} + L_\chi^2 \nu^2 \frac{1}{r}\frac{d}{dr}\rho_{\chi\chi} \right] \qquad (2.2.3)$$

where $\rho_{\psi\psi}$ and $\rho_{\chi\chi}$ are autocorrelation functions for stream functins ψ and velocity potential χ, respectively (see e.g. Daley, 1991). L_ψ and L_χ are corresponding the length scales. A ratio between the divergent and total wind "error" kinetic energy is given by:

$$\nu^2 = \frac{E_\chi^2 / L_\chi^2}{E_u^2}. \qquad (2.2.4)$$

The parameter ν^2 is a measure of divergence in $\rho_{ll}(r)$ and $\rho_{tt}(r)$. When $\nu^2 = 0$ then flow is completely non-divergent and when $\nu^2 = 1$ the flow is irrotational. The observational study shown that reasonable choice for ν^2 is 0.1 and 0.2 what means that rotational flow in atmosphere prevails in comparison with divergent one (Daley, 1991).

In Figure 8 equations (2.2.2-2.2.3) are used to plot the autocorrelations $\rho_{ll}(r)$ and $\rho_{tt}(r)$ for three values of ν^2= 0.0, 0.5 and 1.0. In this figure also $L_\psi = L_\chi = 1$and for calculation of $\rho_{\psi\psi}$ and $\rho_{\chi\chi}$ a model of the form

$$\rho_B(r) = \left(1 + \frac{r}{L}\right) e^{-r/L}, \qquad (2.2.5)$$

have been used, where $\rho_B(r)$ is referred to forecast background (B) positive everywhere. According to Daley (1991) the second correlation model that has been used frequently for the forecast background is

$$\rho_B(r) = \exp\left(\frac{-r^2}{2L^2}\right). \qquad (2.2.6)$$

The behaviour $\rho_{ll}(r)$ and $\rho_{tt}(r)$ in non divergent and irrotational case can be explained by Figure 9 in which a) shows a nondivergent flow and b) an irrotational flow. The iso lines in a)/b) are lines of constant stream function/velocity potential with values increasing form the centres. The flow in a) is counter clockwise around centre ψ_0 and in b) is directed outward from the centre χ_0. In each case, five values of the longitudinal component *l* and transverse component *t* are shown at the same straight line. It is clear that for the nondivergent flow, their effective correlation length is shorter for *t* than it is for *l,* the reverse is true for the irrotational case (see Daley, 1991; Hollingsworth and Lönnberg, 1986).

The autocorrelations $\rho_{uu}(r,\phi)$, $\rho_{uv}(r,\phi)$ and $\rho_{vv}(r,\phi)$ can be calculated from $\rho_{ll}(r,\phi)$ and $\rho_{tt}(r,\phi)$. Under isotropic conditions,

$$\rho_{uu}(r,\phi)=\rho_{ll}(r)\cos^2\phi+\rho_{tt}(r)\sin^2\phi \qquad (2.2.7)$$

$$\rho_{uv}(r,\phi)=\rho_{vu}(r,\phi)=(\rho_{ll}(r)-\rho_{tt}(r))\sin\phi\cos\phi \qquad (2.2.8)$$

$$\rho_{vv}(r,\phi)=\rho_{ll}(r)\sin^2\phi+\rho_{tt}(r)\cos^2\phi \qquad (2.2.9)$$

Note that $\rho_{vv}(r,\phi)=\rho_{uu}(r,\phi+\pi/2)$. The values of $\rho_{uu}(r,\phi)$, $\rho_{uv}(r,\phi)$ and $\rho_{vv}(r,\phi)$ are plotted in Figure 10 for ν^2=0 (nondivergent) as function of r/L_ψ and ϕ. Positive contours are solid and negative contours are dashed. Horizontal scale is indicated under $\rho_{vv}(r,\phi)$correlation. Correlation patterns shown are frequent because divergence component of the atmospheric flow is usually smaller than rotational component as mentioned before (see also Daley, 1991).

From this it can be concluded that upper-air wind measurement at a location has implication on wind filed objective analysis at least thousand kilometres from that position. Thus upper-air measurement of wind at Dubrovnik has contribution to wind field objective analysis in a wider region and on such a way has significant influence on weather forecast in Adriatic area and wider.

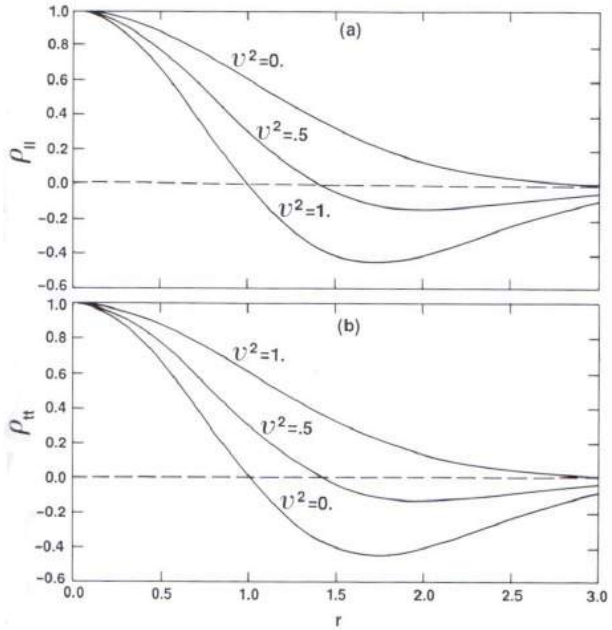

Figure 8 Longitudinal (a) and transversal (b) wind autocorrelation as a function of *r* (10^3 km) for the correlation model (2.2.5). (after Daley, 1991)

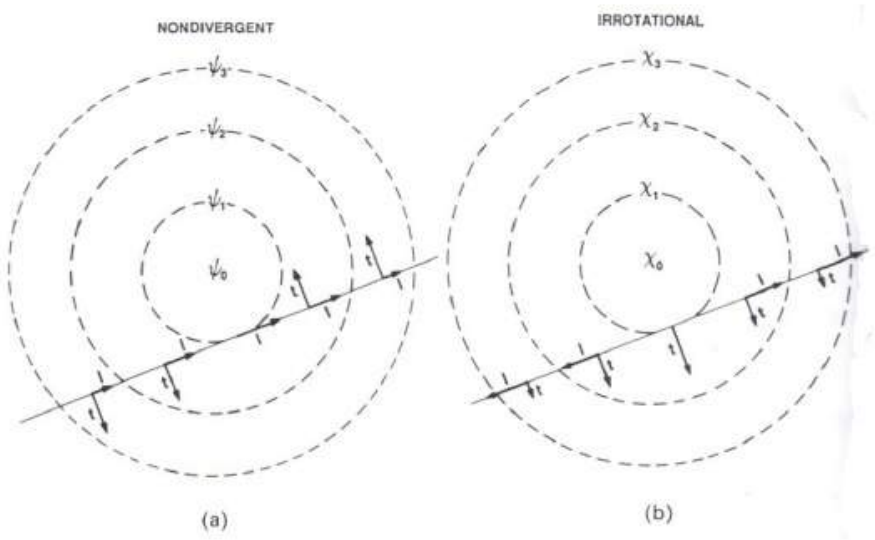

Figure 9 Nondivergent (a) and irrotational (b). Iso lines (a)/(b) are lines of constant Stream functions/velocity potential with an increasing outward from the centre (after Daley, 1991).

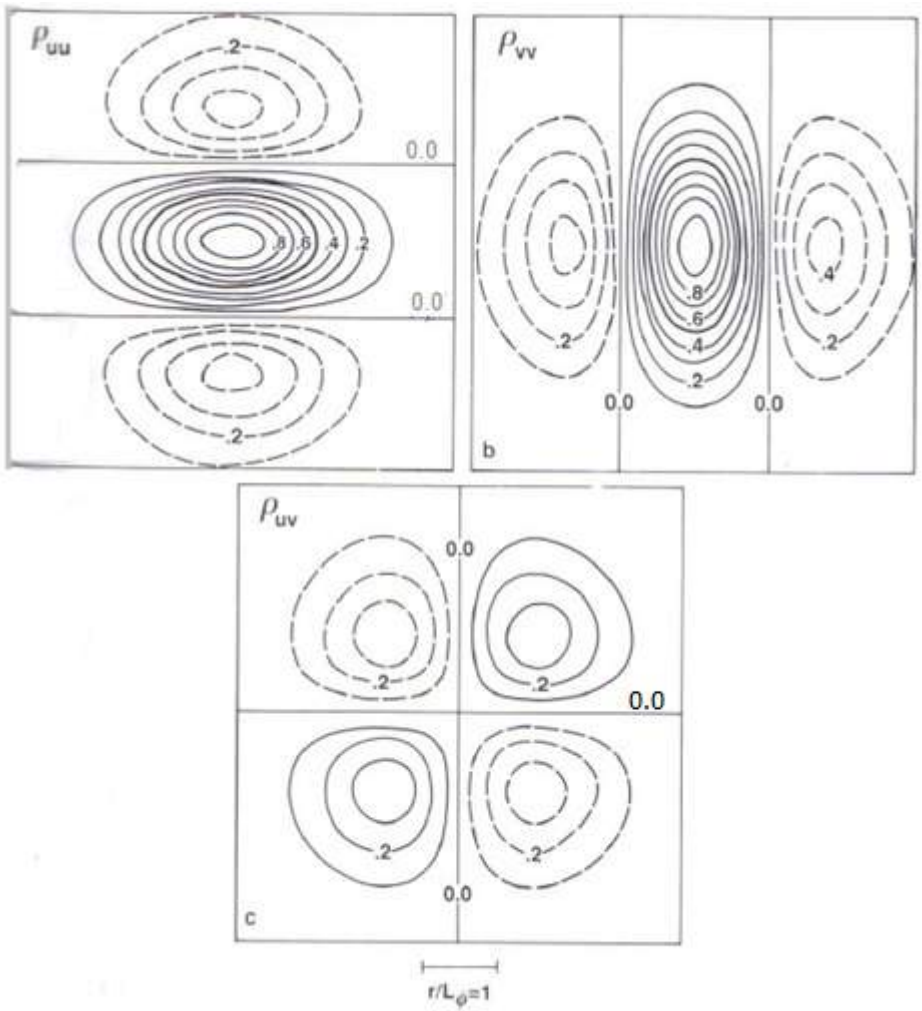

Figure 10 a) $\rho_{uu}(r,\phi)$, b) $\rho_{vv}(r,\phi)$ and c) $\rho_{uv}(r,\phi)$ for the nondivergent isentropic flow for the correlation model (2.2.6). (after Daley, 1991).

3 Weather Research and Forecasting (WRF) atmospheric mesoscale model

3.1 General characteristics

The Weather Research and Forecasting (WRF) model is a numerical weather prediction (NWP)and atmospheric simulation system designed for both research and operational applications.WRF is supported as a common tool for the university/research and operational communities to promote closer ties between them and to address the needs of both. The development of WRF has been a multi-agency effort to build a next-generation meson scale forecast model and data assimilation system to advance the understanding and prediction of meso scale weather and accelerate the transfer of research advances into operations. The WRF effort has been a collaborative one among the National Centre for Atmospheric Research's (NCAR) meso-scale and micro-scale Meteorology (MMM) Division, the National Oceanic and Atmospheric Administration's(NOAA) National Center for Environmental Prediction (NCEP) and Earth System Research Laboratory (ESRL), the Department of Defense's Air Force Weather Agency (AFWA) and Naval Research Laboratory (NRL), the Center for Analysis and Prediction of Storms (CAPS) at the University of Oklahoma, and the Federal Aviation Administration (FAA), with the participation of university scientists(Skamarock et al. 2008).

The principal components of the WRF system are depicted in Figure 11. The WRF Software Framework (WSF) provides the infrastructure that accommodates the dynamics solvers, physics packages that interface with the solvers, programs for initialization, WRF-Var, and WRF-Chem. There are two dynamics solvers in the WSF: the Advanced Research WRF (ARW) solver (originally referred to as the Eulerian mass or "em" solver) developed primarily at NCAR, and the NMM (Nonhydrostatic Mesoscale Model) solver developed at NCEP. Community support for the former is provided by the MMM Division of NCAR and that for the latter is provided by the Developmental Test bed Centre (DTC).

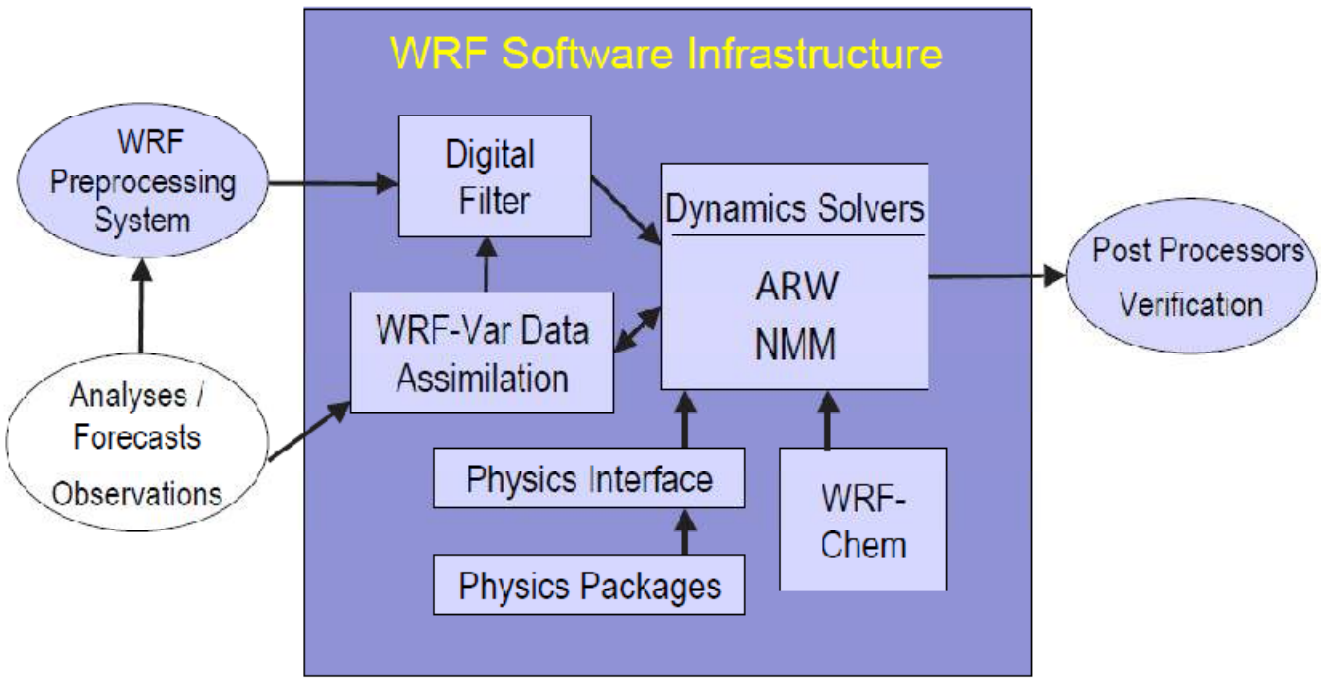

Figure 11 WRF system components (source: Skamarock et al., 2008).

3. 2 Advanced Research WRF

The ARW is the ARW dynamics solver together with other components of the WRF system compatible with that solver and used in producing a simulation. Thus, it is a subset of the WRF modelling system that, in addition to the ARW solver, encompasses physics schemes, numeric's/dynamics options, initialization routines, and a data assimilation package (WRF-Vary). The ARW solver shares the WSF with the NMM solver and all other WRF components within the framework. Physics packages are largely shared by both the ARW and NMM solvers, although specific compatibility varies with the schemes considered. The association of a component of the WRF system with the ARW subset does not preclude it from being a component of WRF configurations involving the NMM solver(Skamarock et al. 2008)..

3.3 Spatial Discretization

The spatial discretization in the ARW solver uses a C grid staggering for the variables as shown in Figure 12. That is, normal velocities are staggered one-half grid length from the thermodynamic variables. The variable indices, (i, j, k) indicate variable locations with (x, y, η) =(iΔx, jΔy, kΔη). We will denote the points where θ is located as being mass points, and likewise we will denote locations where u, v, and w are defined as u points, v points, and w points,respectively. Not shown in Figure 9are the column mass μ, defined at the (i, j) points (mass points) on the discrete grid, the geopotential φ that is defined at the w points, and the moisturevariables$q_m$are defined at the mass points. The diagnostic variables used in the model, the pressure p and inverse density α, are computed at mass points. The grid lengths Δx and Δyare constants in the model formulation; changes in the physical grid lengths associated with the various projections to the sphere are accounted for using the map factors. The vertical grid length Δη is not a fixed constant; it is specified in the initialization. The user is free to specify the η values of the model levels subject to the constraint that η = 1 at the surface, η = 0 at the model top, and η decreases monotonically between the surface and model top. Using these grid and variable definitions, we can define the spatial discretization for the ARW solver (Skamarock et al. 2008)..

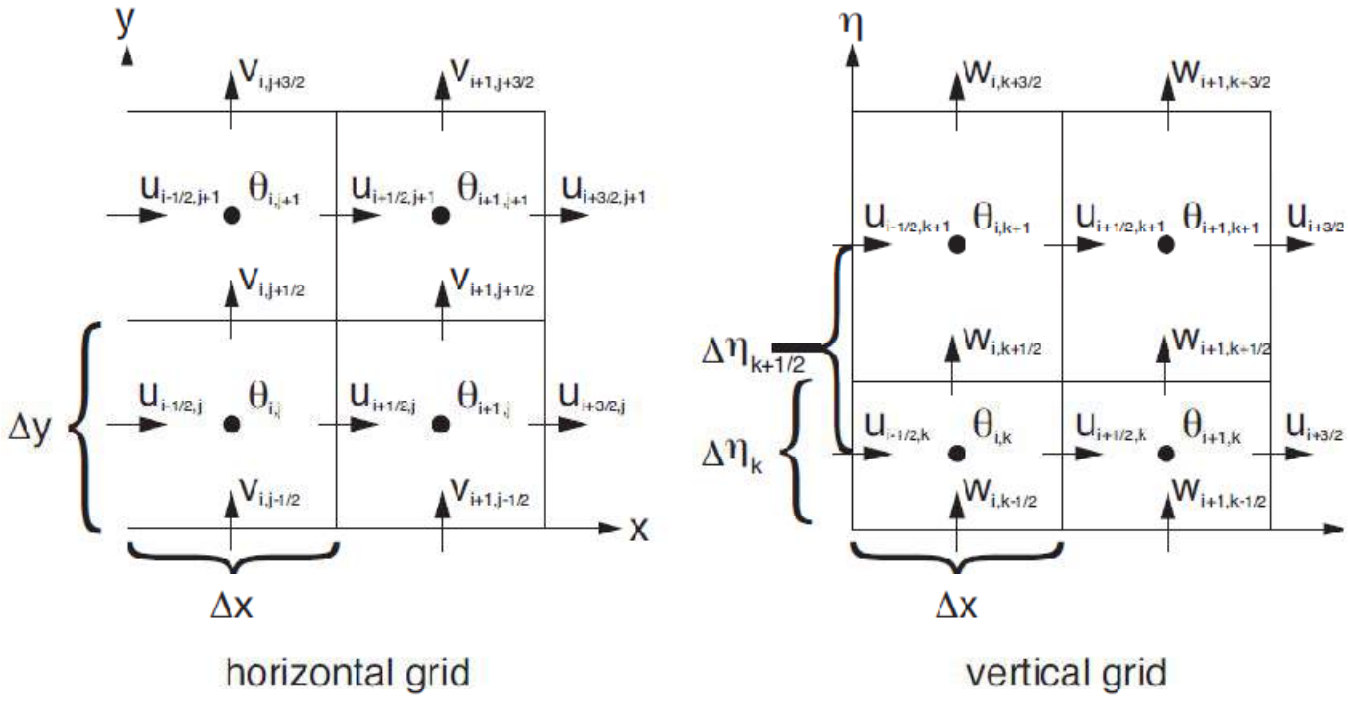

Figure 12 Horizontal and vertical grid at WRF (source: Skamarock et al., 2008).

3.4 Nesting Options

The 1-way and 2-way nesting options refer to how a coarse grid and the fine grid interact. In both the 1-way and 2-way simulation modes, the fine grid boundary conditions (i.e. the lateral boundaries) are interpolated from the coarse grid forecast. In a 1-way nest, this is the only information exchange between the grids (from the coarse grid to the fine grid). Hence, the name 1-way nesting. In the 2-way nest integration, the fine grid solution replaces the coarse grid solution for coarse grid points that lie inside the fine grid. This information exchange between the grids is now in both directions (coarse-to-fine for the fine-grid lateral boundary computational and fine-to-coarse during the feedback at each coarse-grid time step). Hence, the name 2-way nesting (Skamarock et al. 2008)..

3.5 Four-Dimensional Data Assimilation

Four-dimensional data assimilation (FDDA), also known as nudging, is a method of keeping simulations close to analyses and/or observations over the course of an integration. There are two types of FDDA that can be used separately or in combination. Grid- or analysis-nudging simply forces the model simulation towards a series of analyses grid-point by grid-point. Observational or station-nudging locally forces the simulation towards observational data. These methods provide a four-dimensional analysis that is somewhat balanced dynamically, and in terms of continuity, while allowing for complex local topographical or convective variations (Skamarock et al. 2008)..

4 Wind Profiler installation and starting operation

By efforts of DHMZ staff purchase process has been successfully done on 16 April 2019 by signing an Agreement between supplier and DHMZ. About a month latter expert team from supplier came to install wind profiler at Dubrovnik weater station together with DHMZ staff. The installation lasted from 21 to 29 May 2019 (Figures 13 and 14). A training has been done by supplier for a number of DHMZ technical staff. Currently, wind speed and direction data are available each 15 minutes up to about 4 to 7 kilometrs above ground. These data are, since 28 May 2019, operationally available to all AdriaMore Project Partners (PPs) as well as to World Meteorological Organization (WMO) members via WMO and EUMETNET telecommunication lines in BUFR format (figure 15). Maintenance of the wind profiler will be done by DHMZ. Available data are in two wind profiler modes: the first up to 3 km heights above ground and the second up to 7 km above ground.

Figure 13 Instalation of wind profiler at GMP Dubrovnik from 21 to 29 May 2019.

Figure 14The wind profiler instaled at GMP Dubrovnik (on the right side of photo).

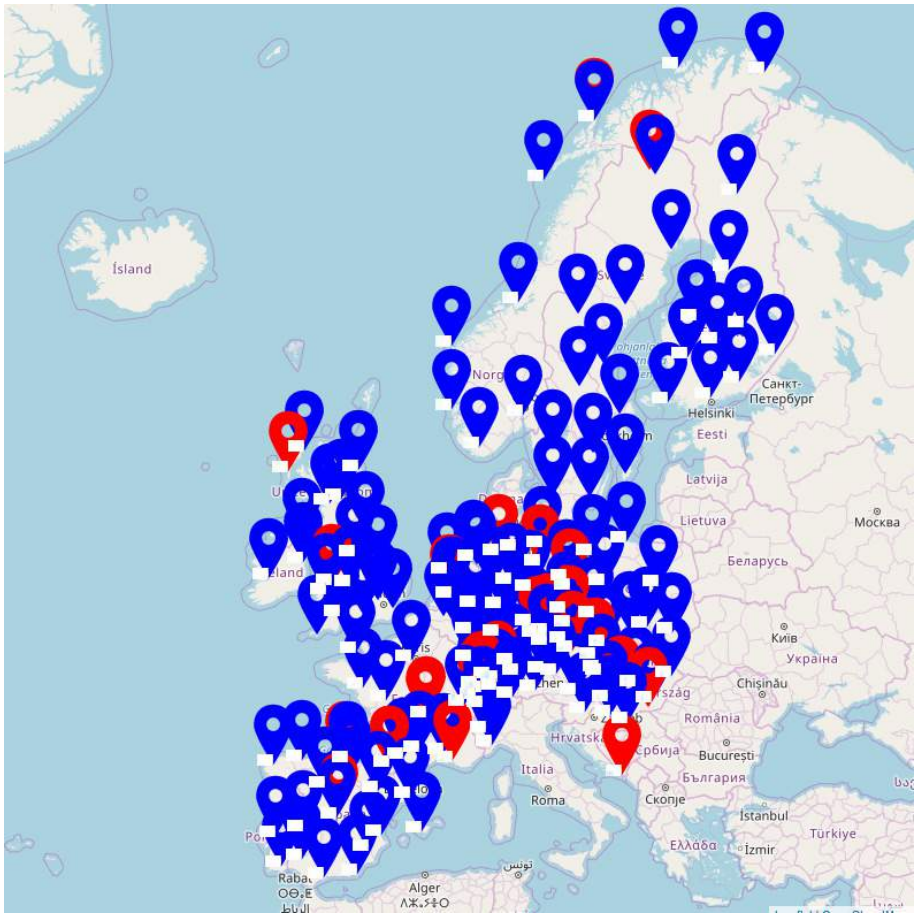

Figure 15 Wind vertical profile observation by weather radars (blue colour) and wind profilers (red colour) within e-profile of EUMTNET (source: https://e-profile.eu/#/wp_profile).

On Figure 16 a vertical profile of wind at Dubrovnik weather station (latitude: 42.64 N; longitude: 18.08 E; elevation: 52m) for 29 May 2019 which has been observed by “high mode” wind profiler. It is obvious from the Figure 16 that height of upper air wind observation varies from 4k to 7 km depending on state of atmosphere (up to 4 km in clear air and beyond in precipitation). Colours indicate wind speed categories indicated on the right side of the figure.

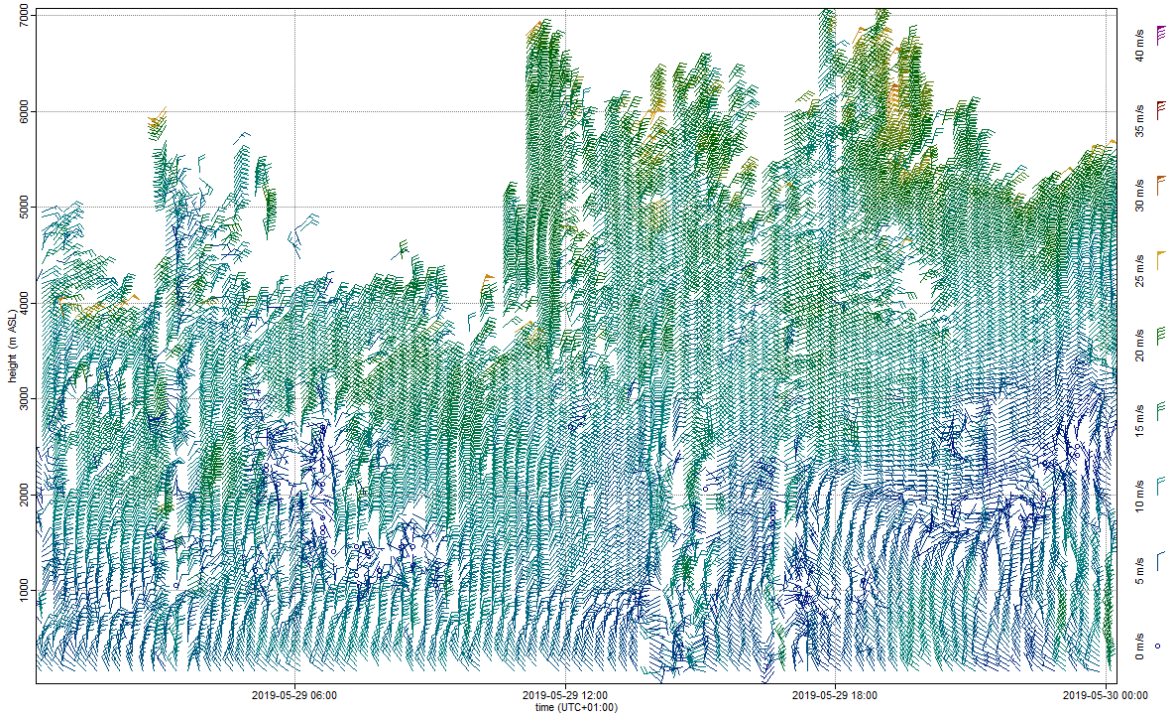

Figure 16 Vertical profile of wind at Dubrovnik weather station for 29 May 2019 observed by wind profiler (high mode and wind vector azimuth).

5 Reanalysis of ERA5[3] wind data for Dubrovnik region and interpretation of autocorrelation wind component functions

Wind speed, wind dirrection and wind gusts (in mph) at 10 m level above ground in wider area of Europe for 29 May 2019 at 00 UTC is presented in Figure 17. Zones of severe wind are indicated by colours. In addition to the Northern Atlantic and the Northern Europe the zones of severe winds are present also in Meditteranean region including the Southern Adriatic. At the same time a configuration of wind field on the level of 500 hPa constanr air pressure surface is represented in Figure 18. The strongest north-westerly wind was above the Western Europe and near westerly wind over the Southern Italy and Greece, Scandinavia and over the parth North-Western Rusia. Cited configuration of wind filed can help an interpretation of *u* and *v* wind component configurations represented in Figures 19 – 24. Wind configuration at the 500 hPa constant air pressure surface is related to large troght with axes from Norway to Genoa Bay.

u-componnet of wind at 500 hPa constant air pressure surface are represented in Figures 19 to 21. There are two poles of u-component wind speed in the area considered: one positive centre in Western Meditteranean and a secondary northerly ofit for 29 May 2019. These two centers were slowly moved to the east next days i.e. 30 and 31 May 2019. Thus, positions of two ceters were moved toward Central Mediterranean and Central Europe, respectively. These moving was rather persistent and typical patterns in *u* and *v* wind components can be recognised. As a results a typical autocorrelation patterns can be recognised for compnents of wind filed as it was shown in Chapter 2, especialy in Figure 10. Thus, it was shown (e.g. Daley, 1991), that an observation of upper air wind has an influnce on objective analysis of wind components more than thousand kilometres far away from location of observation, Consequently, observation of upper air wind by wind profiler at Dubrovnik has signicifant contribution to objective analysis of wind field and weather forecast in the region i.e. data assimilation for forecasting numerical models including the WRF.

[3]ECMWF (Euroepan Center for Medium Range Weather Forecasts) Reanalysis of 5-th Generation

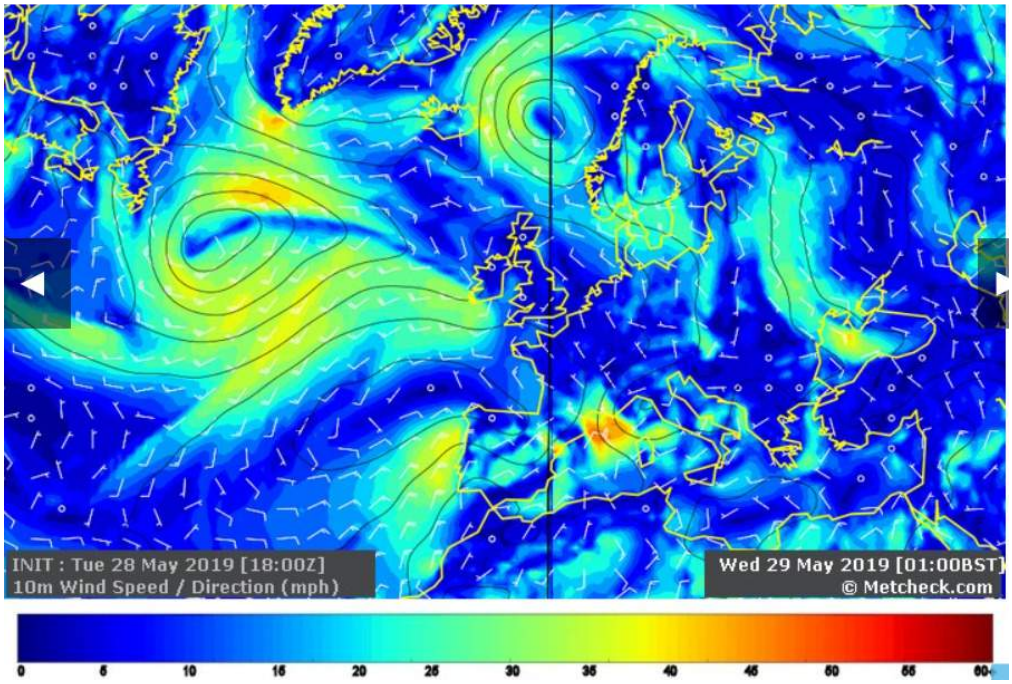

Figure 17 Wind speed, wind dirrection and wind gusts at 10 m level above ground in wider area of Europe for 29 May 2019 at 00 UTC (source: http://www.metcheck.com/WEATHER/gfscharts_archive.asp)

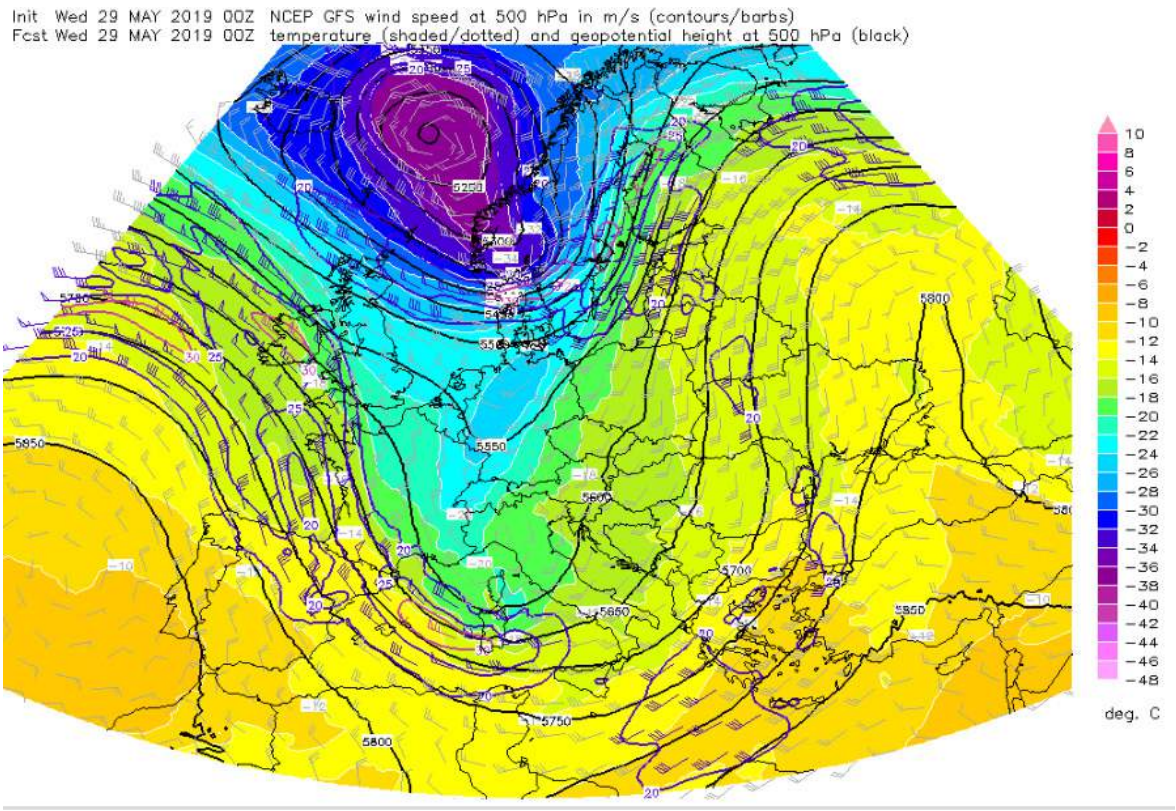

Figure 18 Wind at 500 hPa surface over Europe for 29 May 2019 at 00 UTC,indicated by barbs (source: **http://www.estofex.org/**)

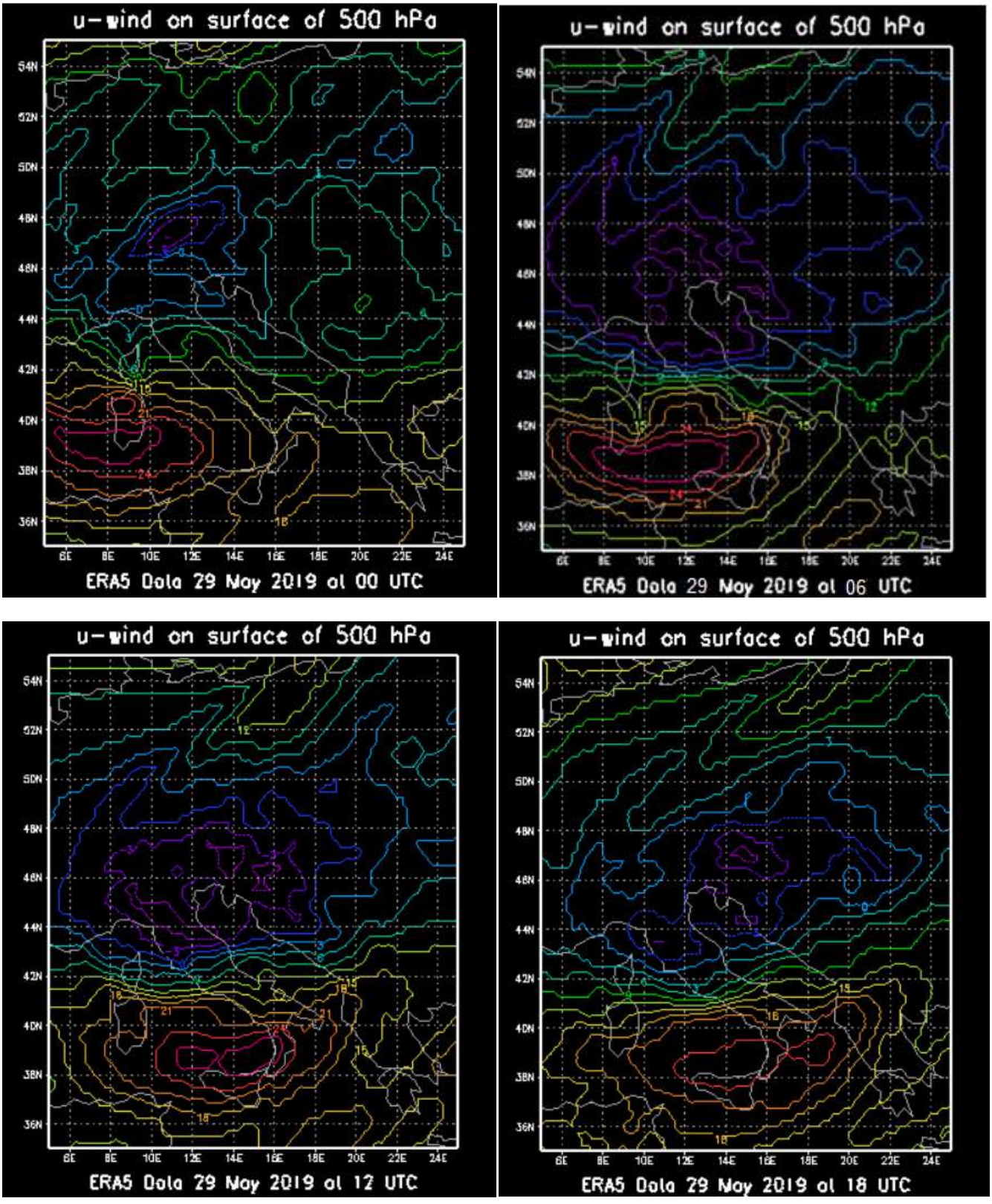

Figure 19 Spatial distribution of u-component (metres per second) of wind on 500 hPa constant pressure surface for central and southern Europe for 29 May 2019.

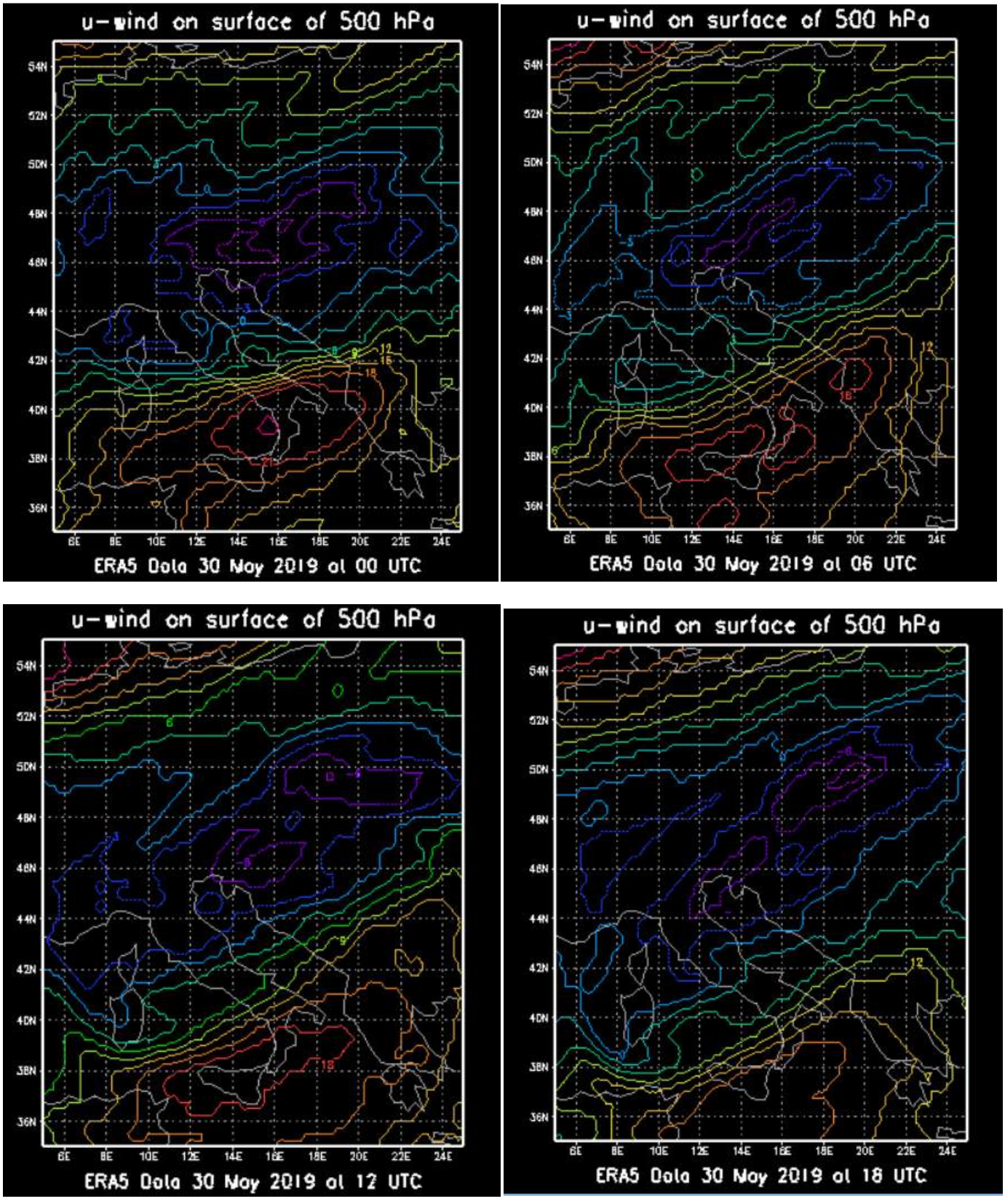

Figure 20 Spatial distribution of u-component (metres per second) of wind on 500 hPa constant pressure surface for central and southern Europe for 30 May 2019.

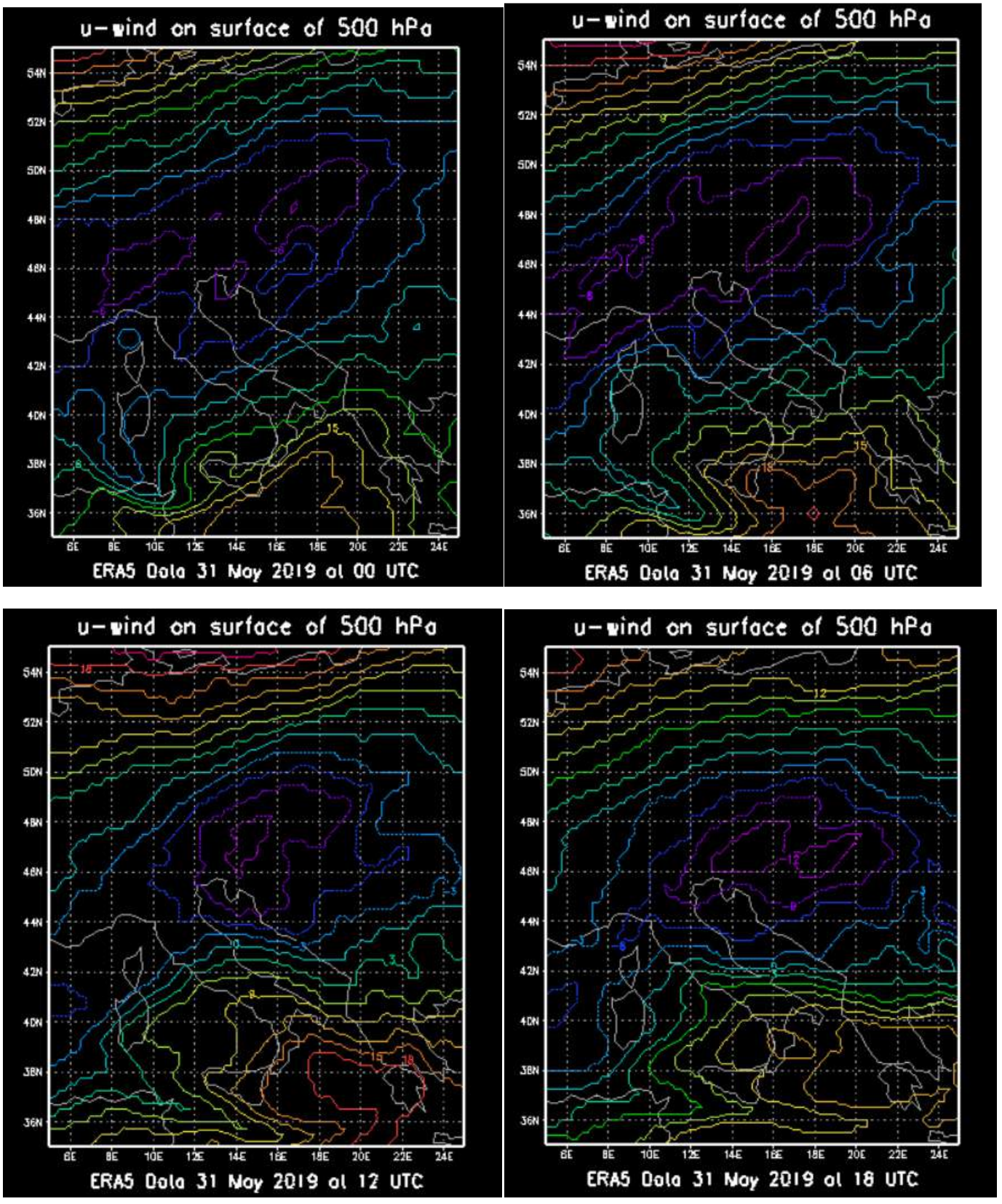

Figure 21 Spatial distribution of u-component (metres per second) of wind on 500 hPa constant pressure surface for central and southern Europe for 31 May 2019.

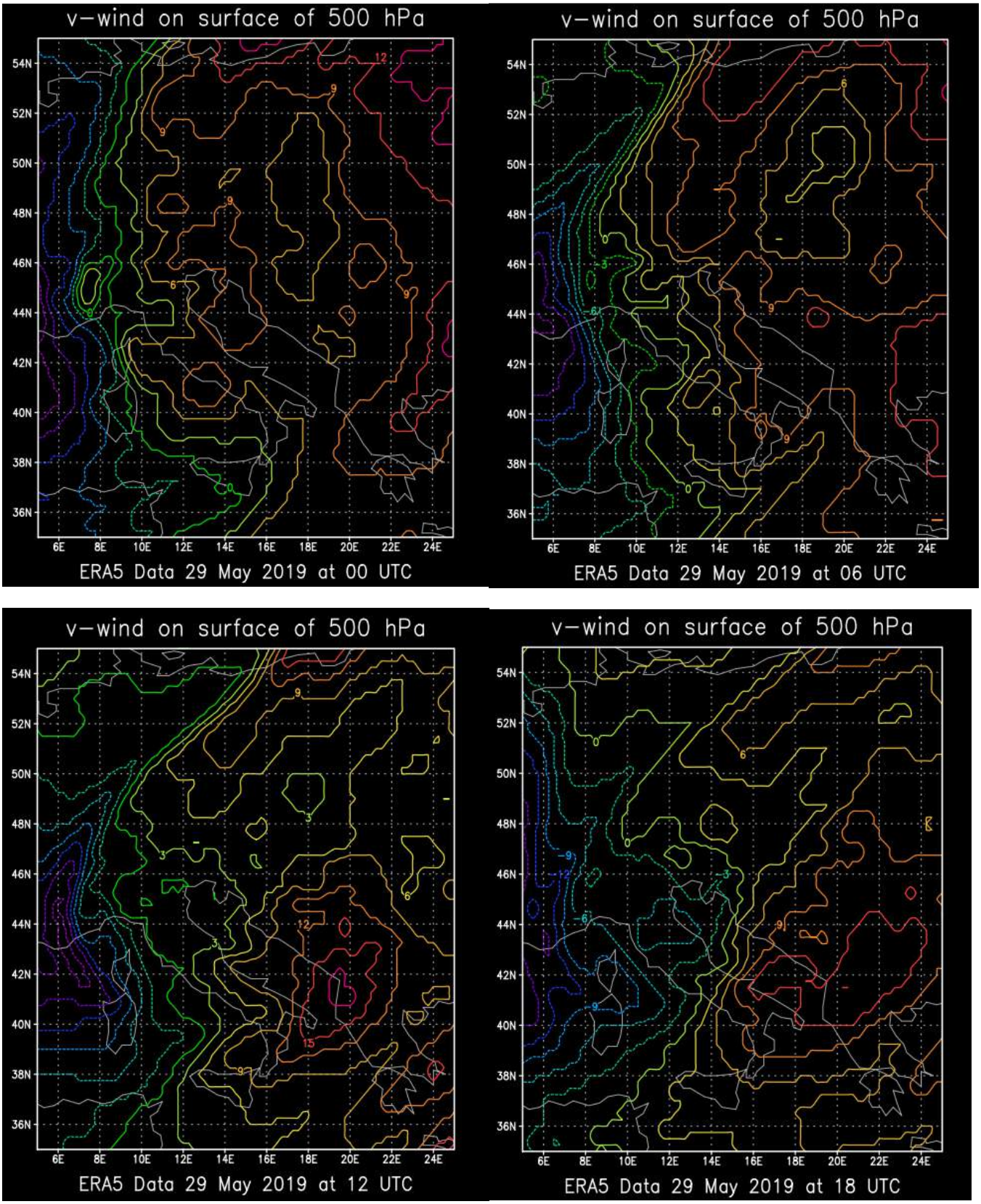

Figure 22 Spatial distribution of v-component (metres per second) of wind on 500 hPa constant pressure surface for central and southern Europe for 29 May 2019.

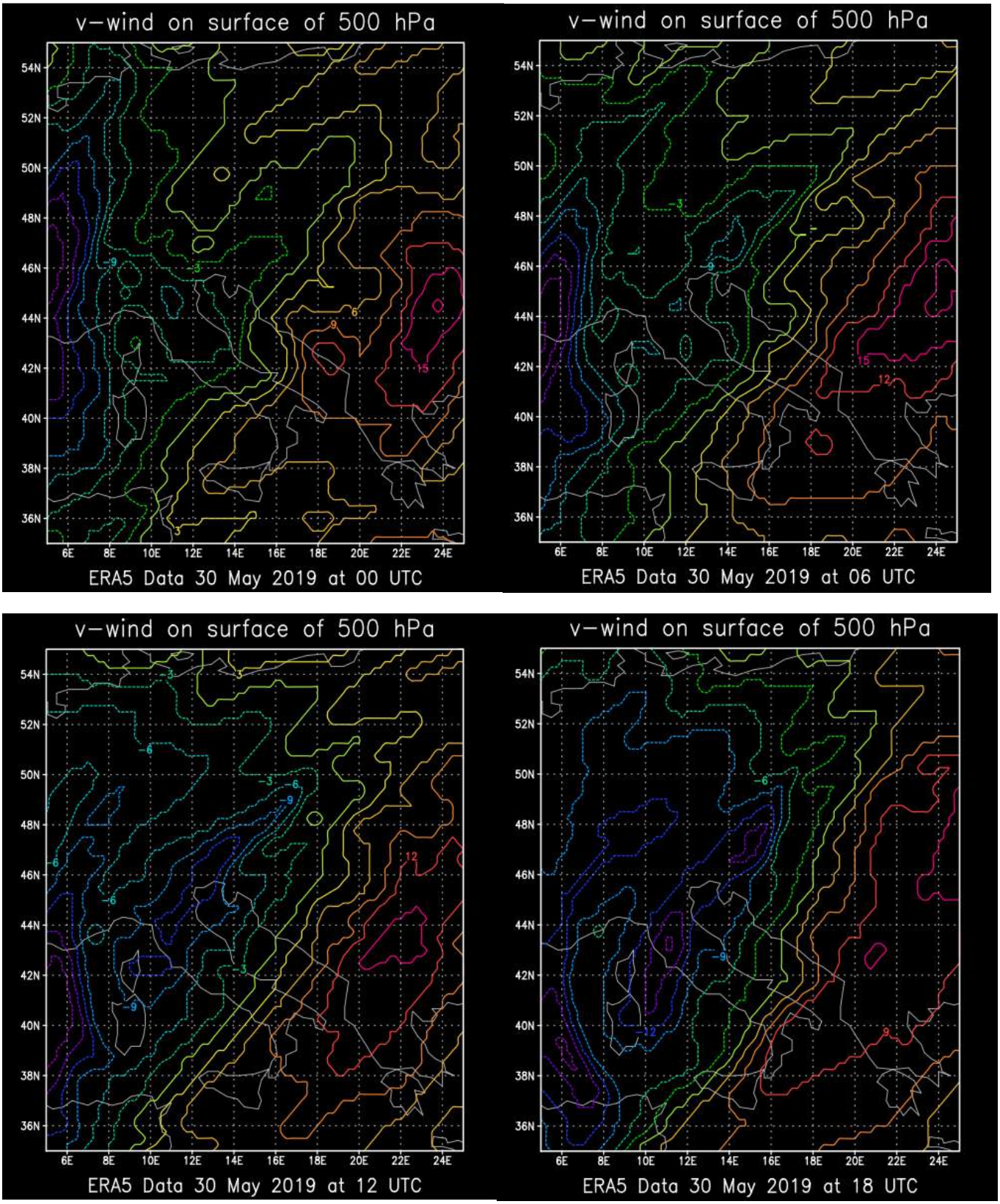

Figure 23 Spatial distribution of v-component (metres per second) of wind on 500 hPa constant pressure surface for central and southern Europe for 30 May 2019.

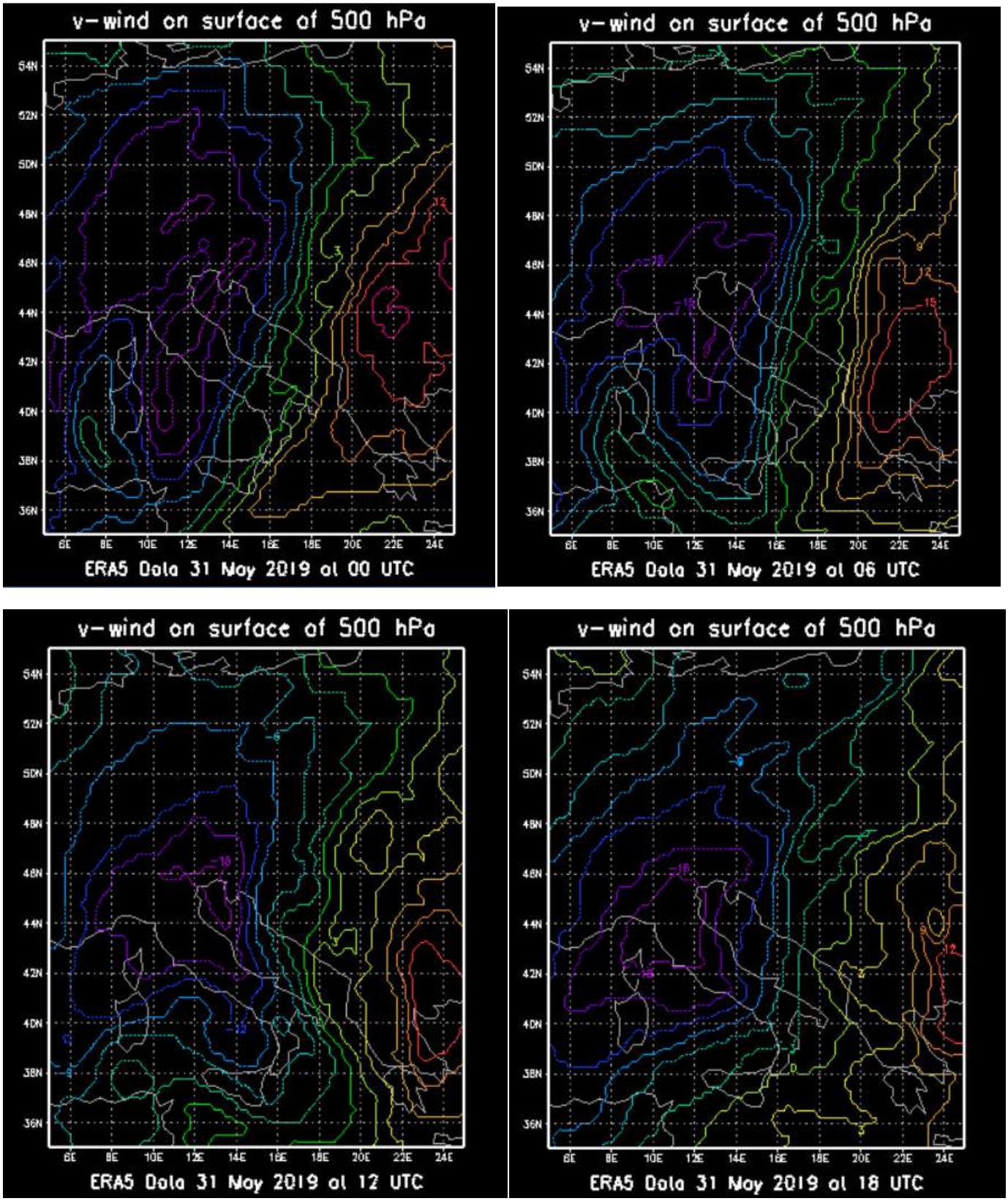

Figure 24 Spatial distribution of v-component (metres per second) of wind on 500 hPa constant pressure surface for central and southern Europe for 31 May 2019.

6 Comparison of the WRF mesoscale model outputs with and without upper wind data observed by wind profiler at Dubrovnik

Two case studies have been selected for comparison of the WRF model outputs with and without assimilation of upper air wind data of wind profiler at Dubrovnik weather station. The first is 1 June 2019 as the coldest day in that June and the second is 28 June 2019 the second as the warmest day in that June (see Figure 25).

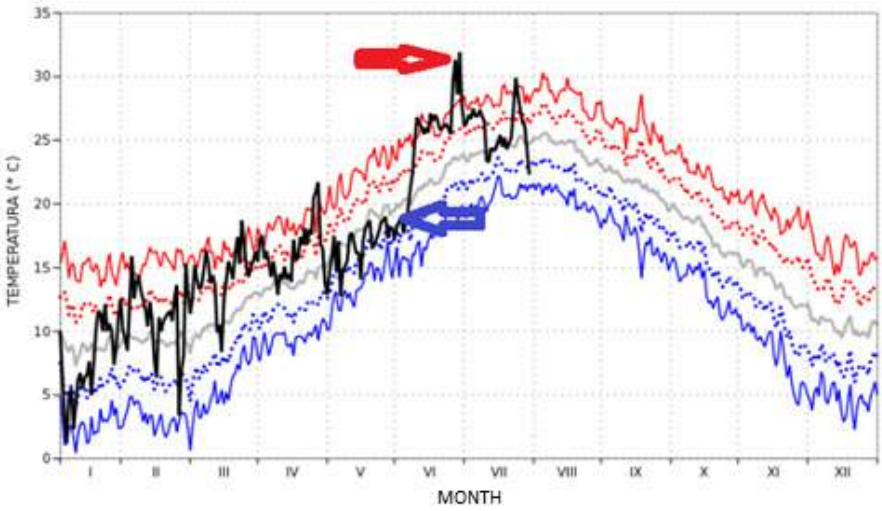

Figure 25 Comparisin of average daily 2m height air temperature by reference period 1961-1990 averages of corresponding daily air temperature decriesd for one (dot red line) and two standard deviations (solid red line) and decrised for one (dot blue line) and two standard deviations (soild blue line).
(source: www.meteo.hr)

6.1 1 June 2019 case study

Day 1 June 2019 was the coldest day in June 2019 at Dubrovnik weather station i.e. about one standard deviation colder than reference period 1961-1990 average. A cut of is visible in the field of 500 hPa surface heights in Figure 26 over Adriatic Sea. A core of relative cold air circulate over that area. A weak hydrostatic intability is visibly over Adriatic sea (Figure 27).

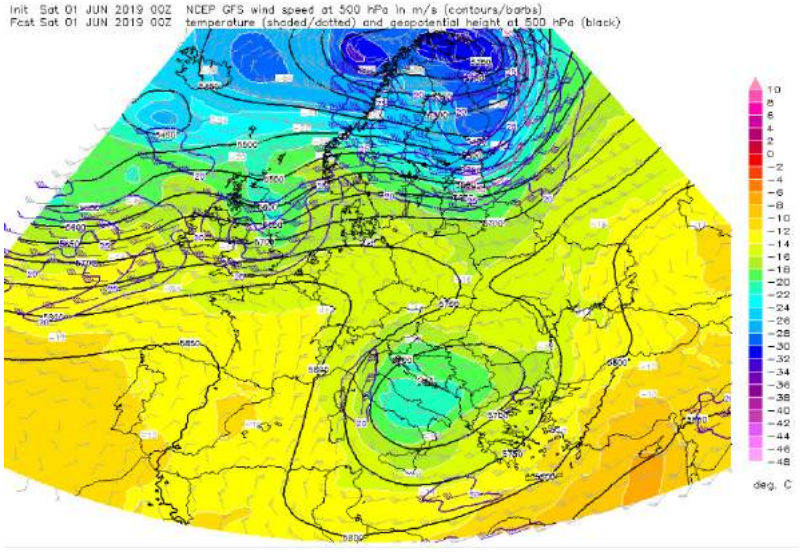

Figure 26 Distribution of 500 hPa constant air pressure surface heights for 1 June 2019 at 00 UTC.
(source: http://www.estofex.org/)

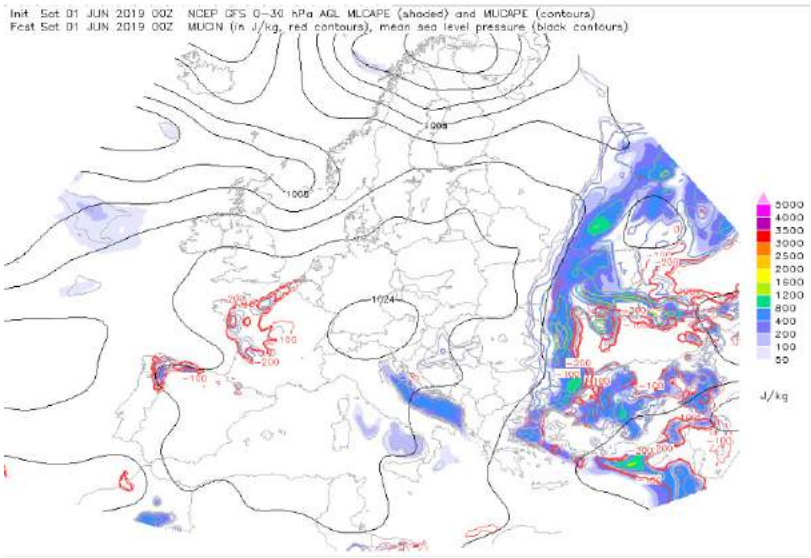

Figure 27 Distribution of MLCAPE[4] (shaded), MUCAPE[5] (contours), MUCIN[6] (red contours) and sea level pressire (black contours) on 1 June2019 at 00 UTC.
(source: http://www.estofex.org/)

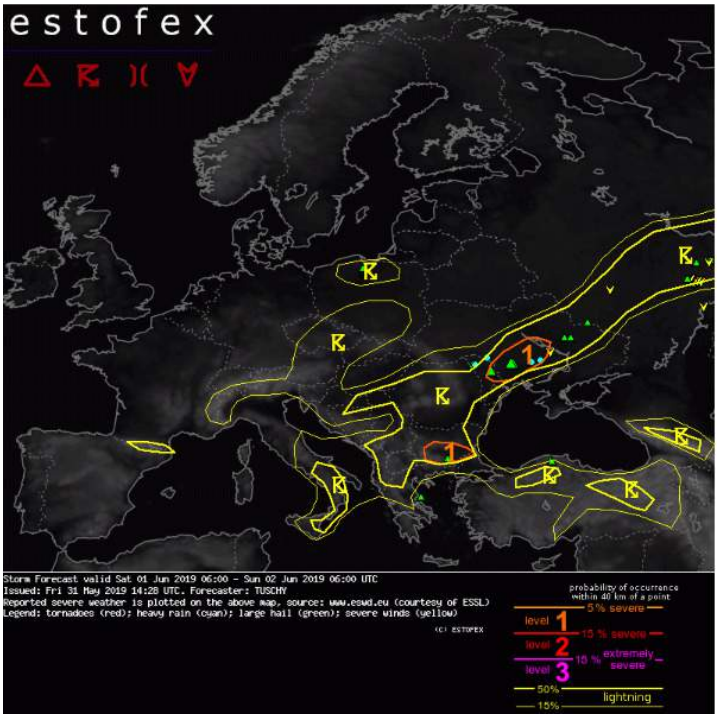

Figure 28 Storms forecast valid from Sat. 1 June 2019 06:00 to Sun. 2 June 2019 06:00.
(source: http://www.estofex.org/)

Cited form Estofex portal:

"Storm Forecast
Valid: Sat 01 Jun 2019 06:00 to Sun 02 Jun 2019 06:00 UTC (Figure 28)

[4]Mixed layer convective available potential energy
[5]Most unstable convective available potential energy
[6]Unstable air parcel Convective Inhibition

Issued: Fri 31 May 2019 14:28
Forecaster: TUSCHY

A level 1 was issued across S-Bulgaria mainly for large hail.

A level 1 was issued across parts of Moldova and S-Ukraine mainly for large hail and a low-end tornado threat.

SYNOPSIS

On the synoptic-scale not much change to talk about. Progressive flow regime continues over N-Europe with wave-train of small-amplitude troughs racing east. Those waves miss connection to the quasi-stationary upper trough over S-Italy. This trough remains concreted in-between two broad ridges over SW/SE Europe.

Yesterday's wavy front over Moldova/Ukraine into Russia seems to shift a bit to the SE (partially outflow driven by yesterday's activity), but overall not much regional change is forecast.

DISCUSSION

... E/SE-Europe ...

We desist from discussing certain areas due to the diffuse nature of synoptic-scale forcing. Departing mid-level short-wave trough over Romania drifts W and deamplifies, leaving a rather smooth SW-erly flow regime behind, which affects most of Bulgaria, Romania into Moldova. Similar ingredients to yesterday are forecast with moderate to rich low-tropospheric moisture beneath meagre mid-level lapse rates causing MLCAPE to reside in the 500-1000 J/kg range. DLS increases from N to S with peak values around 15 m/s along the border of Bulgaria/Greece.

Romania and Moldova are probably influenced by the overnight convection with residual showers/thunderstorms and lots of cloudiness. Despite a gradual weakening/advection to the N, diabatic heating remains questionable for CI during the afternoon. Latest idea is to see some re-development along outflow boundaries and along the orography until the evening with locally heavy rain the main risk. Can't exclude isolated hail in strongest cells over S/far E Romania, but weak shear precludes a severe risk.

Bulgaria will see better diabatic input and we added a level 1 for S-Bulgaria. A few multicells with large hail are possible.

Another level 1 area was added for the S-Ukraine, where MLCAPE in excess of 1000-1500 J/kg overlaps with marginal DLS values (at or below 10 m/s). However, amount of CAPE in the hail growth zone indicates a risk of large hail with initiating storms. In addition better directional LL shear next to the front may yield a non-zero tornado risk. Overall this is enough for a level 1. Further east, bad timing of early CI (limited diabatic heating until the early afternoon) and placement beneath the ridge preclude a level 1 for now.

Elsewhere, gusty winds and grapple/isolated hail accompany strongest activity."

6.2 28 June 2019 case study

Day 28 June 2019 was the warmest day in June 2019 at Dubrovnik weather station i.e. about two standard deviations warmer than reference period 1961-1990 average. A ridge is visible in the field of 500 hPa

surface heights in Figure 29 over Adriatic Sea. A relative cold air circulates over North Eastern Europe. A strong hydrostatic intability is visibly over Adriatic sea (Figure 30).

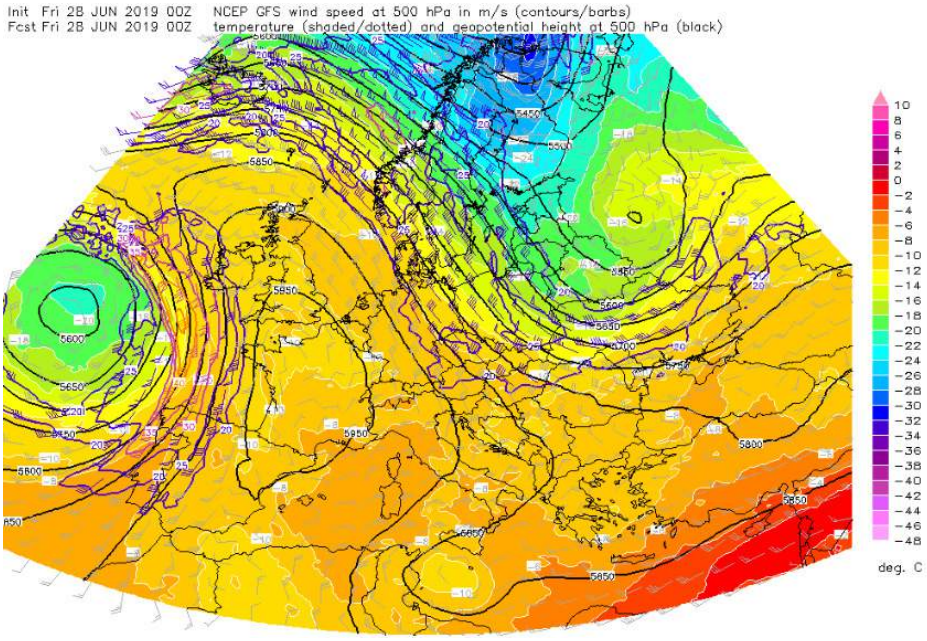

Figure 29 Distribution of 500 hPa constant air pressure surface heights for 28 June 2019 at 00 UTC. (source: **http://www.estofex.org/**)

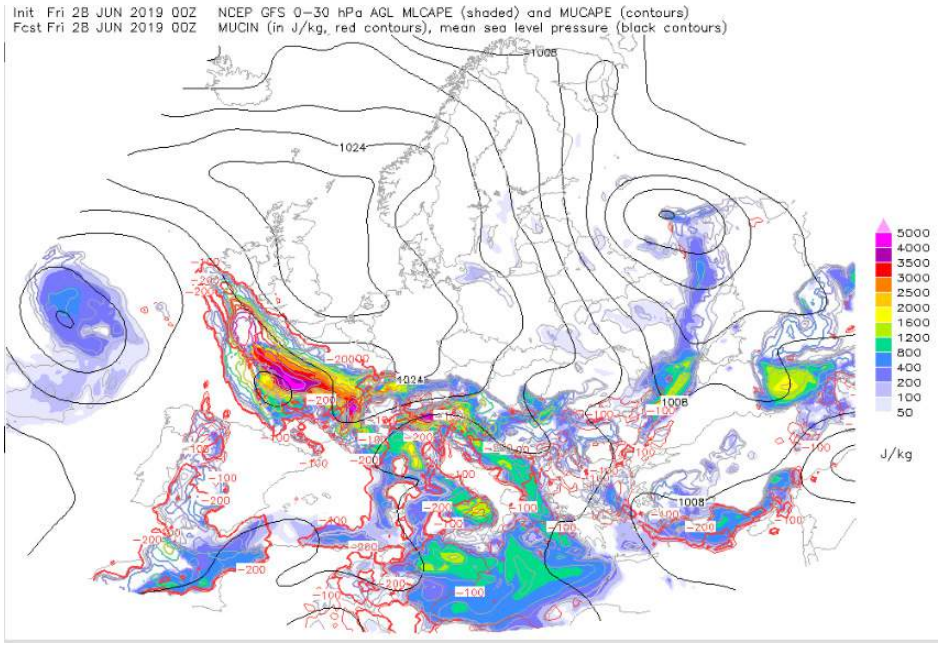

Figure 30 Distribution of MLCAPE (shaded), MUCAPE (contours), MUCIN (red contours) and sea level pressire (black contours) on 28 June 2019 at 00 UTC.
(source: **http://www.estofex.org/**)

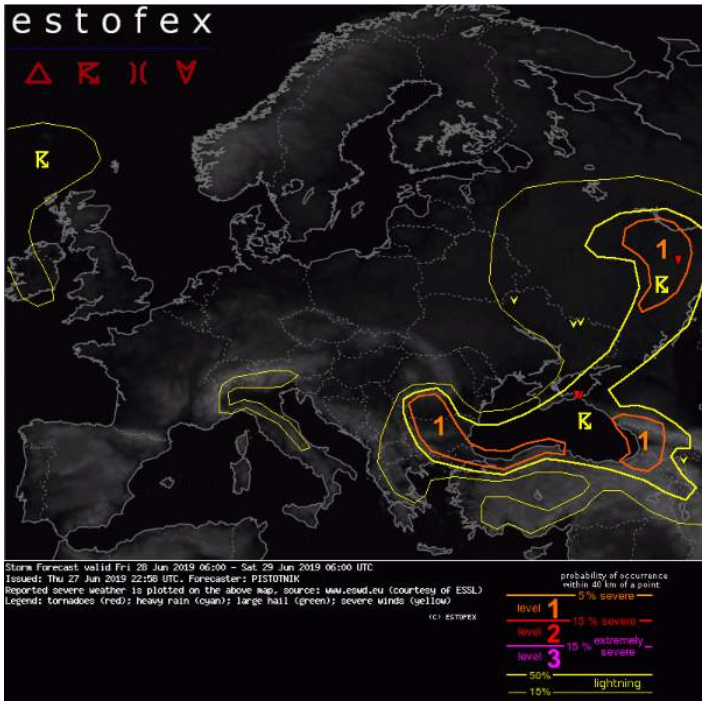

Figure 31 Figure 24 Storms forecast valid from Fri. 28 June 2019 06:00 to Sat. 29 June 2019 06:00.
(source: http://www.estofex.org/)

Cited form Estofex portal:

"Storm Forecast
Valid: Fri 28 Jun 2019 06:00 to Sat 29 Jun 2019 06:00 UTC (Figure 31)
Issued: Thu 27 Jun 2019 22:58
Forecaster: PISTOTNIK

Level 1 areas are issued for parts of SW Russia, Georgia, N Turkey, Bulgaria and S Romania for excessive convective precipitation, large hail and severe convective wind gusts.

SYNOPSIS

An amplified flow pattern covers Europe. A stationary long-wave trough is in place over the Atlantic Ocean, another one amplifies over European Russia and the Ukraine towards Turkey. In-between, a subtropic long-wave ridge stretches from Algeria to the North Sea.

Cooler and drier air floods eastern Europe in the wake of the eastern trough. In contrast, extremely hot air remains in place over Spain, Italy, Switzerland, France and England ahead of the western trough.

DISCUSSION

... SW Russia, Black Sea region, Georgia, N Turkey, Bulgaria and S Romania ...

The cold front of a 990 hPa surface cyclone between Moscow and Nishny Nowgorod moves SE-ward and crosses SW Russia, the Asow and Black Sea. Its tail becomes nearly stationary along the Turkish north coast and over Bulgaria and Romania. A belt of enhanced low-level moisture ahead of the cold front provides CAPE on the order of some hundred J/kg, possibly up to 1000 J/kg, though the model forecast will likely overestimate low-level moisture to some degree (2m dew points in the warm sector were several degrees lower than predicted on Thursday).

Scattered thunderstorms will likely be active throughout the forecast period, most of them in the afternoon. Strong lift ahead of the upper-level trough and moist, only slightly unstable vertical wind profiles point to a primary risk of excessive precipitation, especially near the cyclone's center, where the storm motion is slow. 0-3 km shear between 10 and 15 m/s can support multicellular convection. Moderately large hail and severe wind gusts are therefore also possible with the strongest storms, the former mostly in case of discrete convection and the latter mostly in case a convective line forms at the cold front.

A similar environment of low to moderate CAPE and moderate vertical wind shear exists also ahead of the cold front over NE Turkey, Georgia and the Russian Caucasus region, where the increasing westerly flow pumps Black Sea moisture onshore. Scattered, mostly diurnally driven thunderstorms over the mountains or at the sea breeze front pose a risk of a few flash flood, large hail and downburst events.

... N Italy, Switzerland, France, Celtic Sea, SW England, Ireland towards Faroe Islands ...

A belt of huge CAPE, possibly up to 4000 J/kg (see the Thursday 12z Milan and Cuneo soundings) remains in place where abundant low-level moisture has accumulated under a pronounced elevated mixed layer of Saharan origin. Isolated, short-lived afternoon storms are possible over the Italian mountains, but are not expected to tap into the CAPE reservoir over the adjacent lowlands. Otherwise, the massive capping inversion will still hold.

Robust CAPE of probably more than 1000 J/kg is also advected NW-ward over the Celtic Sea, Ireland and towards the Faroe Island. Strong vertical wind shear and synoptic lift overspread it and would create a favourable environment for severe storms. However, forecast soundings show an impenetrable cap due to the cool sea surface. A rather large low probability lightning area is drawn to account for the possibility of an elevated MCS, which could form in the strong warm air advection regime but is difficult to locate. If it forms, heavy precipitation and large hail are not ruled out."

6.3 Qualitative comparison of the WRF outputs with and without assimilation o upper wind at Dubrovnik

Finaly, a comparison between the WRF outputs with and without assimilation of upper wind for Dubrovnik weather stations has been made. 12h and 24h forecasts of precipitation amounts and 10m wind for two case staidies are considered. Precipitation amount forecats for 1 June 2019 case study are represented in Figure 32. A minor differences between two ways of forecasts can be oserved, more emphasised for 24h precipitation amount forecasts at central Adriatic. In 10m wind field a difference can be observed for two forecasting approach: fo 12h forecast an area of moderate wind is wider in the case when assimilation of upper air wind was made than in the case it was not icluded, but for 24h wind forecasts the result seems as opposite – a wider region of moderate wind speed in the case when upper air wind has not been assimilated (Figure 33). Corresponding forecasts for 28 June 2019 case study are represented in Figures 34 and 35. Again, differences between precipitation amount forecasts are more emphasised in the case of 24h forecasts than for 12h ones. It means, that precipitation forecasts for longer periods could be more and more different (Figure 34). In the case of 10m wind field differences between two way forecasts for 12h and 24h are not obvious (Figure 35).

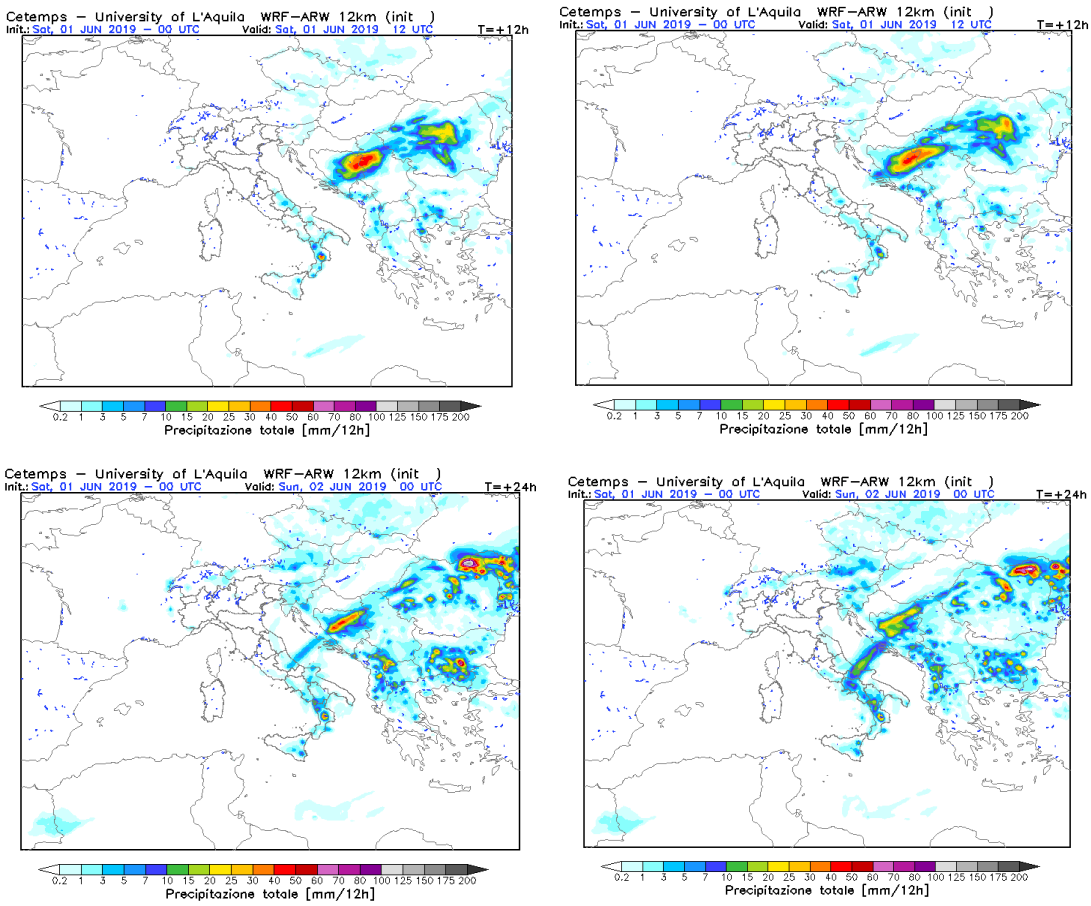

Figure 32 Total 12h and 24h precipitation forecasts for without (left) and with (right) upper wind assimilation at Dubrovnik for 1 June 2019 (source: CETEMPS)

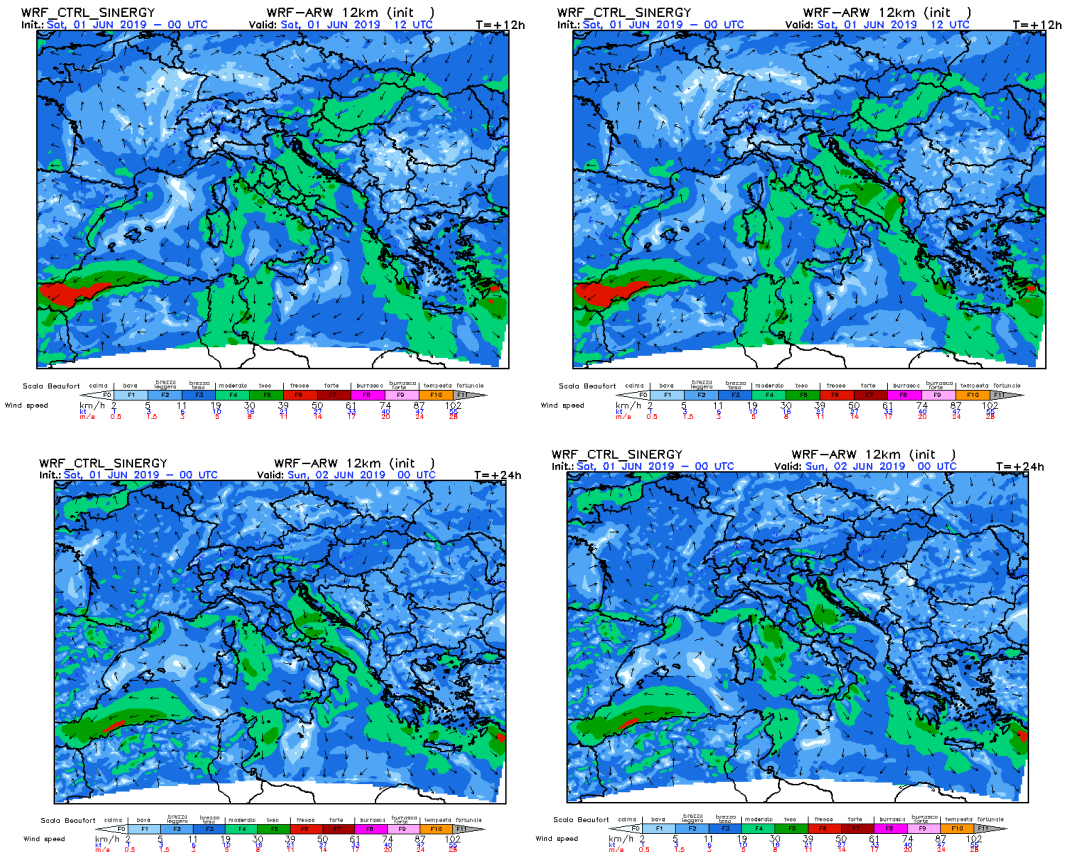

Figure 33 Total 12h and 24h 10m wind forecasts for without (left) and with (right) upper wind assimilation at Dubrovnik for 1 June 2019 (source: CETEMPS).

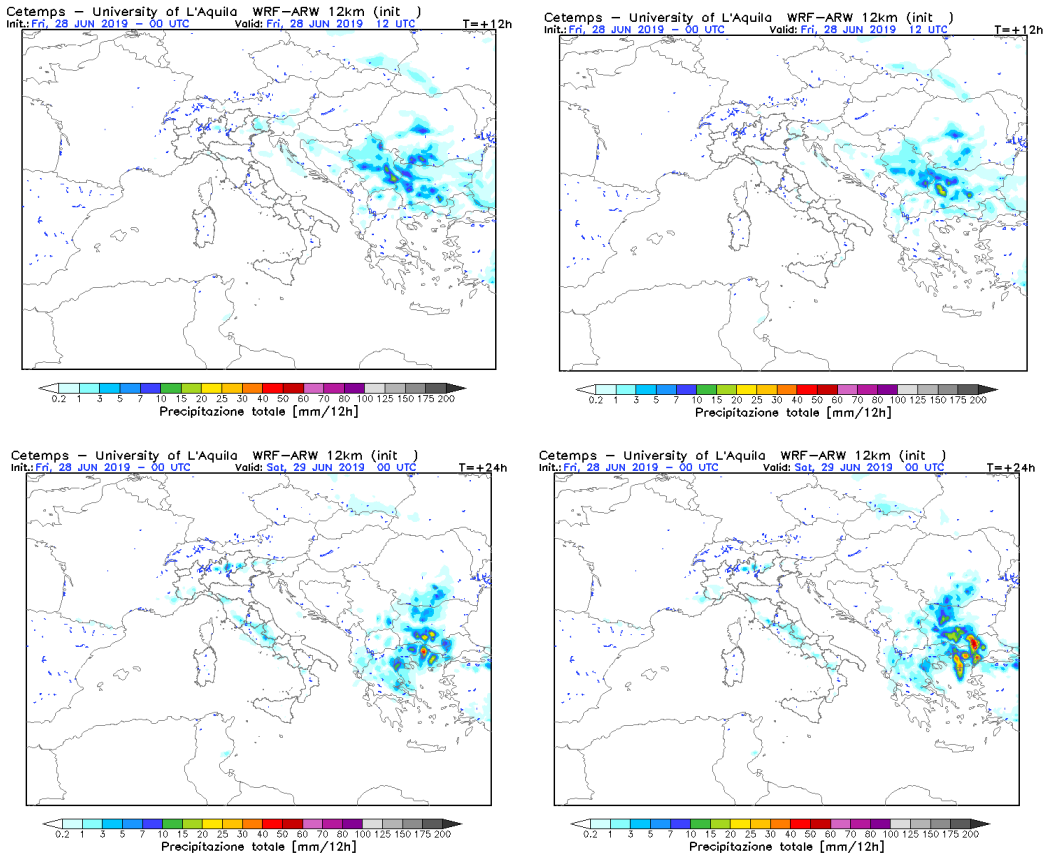

Figure 34 Total 12h and 24h precipitation forecasts for without (left) and with (right) upper wind assimilation at Dubrovnik for 28 June 2019 (source: CETEMPS)

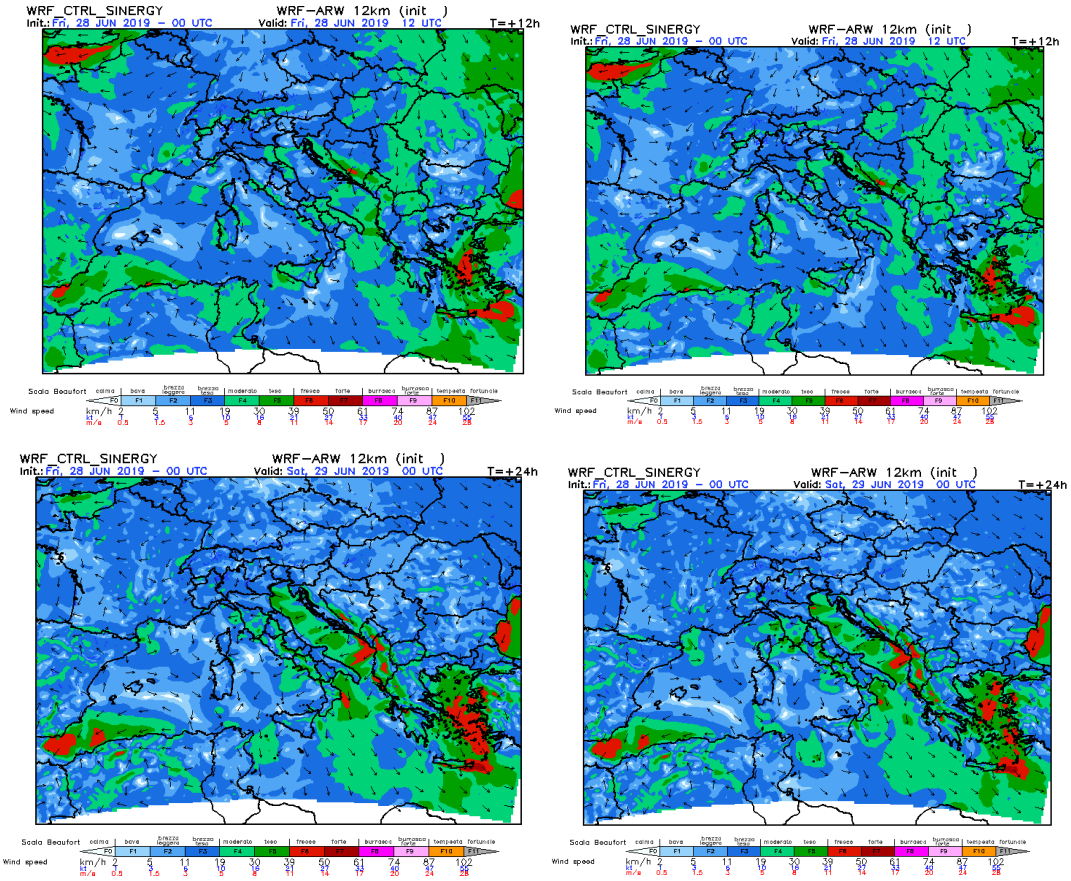

Figure 35 Total 12h and 24h 10m wind forecasts for without (left) and with (right) upper wind assimilation at Dubrovnik for 28 June 2019 (source: CETEMPS).

7. Conclusion

A successful purchase and installation of wind profiler at Dubrovnik weather station has been performed until 28 May 2019 i.e. during the third reporting period of the AdraMORE Project. About one month upper air wind data indicate that mostly observations reach an elevation between 4 to 7 km what was indicated in technical specification of the equipment.

Autocorrelation function analysis indicate that upper air wind components at a location has an influence on wind field interpolation (objective analysis) more than thousand kilometres far from that location. Some kind of interpretation of those theoretical results, confirmed by empirical data, has been shown by representation of wind components on 500 hPa constant air pressure surface for period from 29 to 31 May 2019 for South Eastern Europe each 6-hours. As a consequence of rather persistent wind circulation patterns is a configuration of autocorrelation functions presented in chapter 2 of this report.

Finally, qualitative analysis of the WRF outputs with and without upper air wind assimilation for two case studies has been made for the coldest 1 June and for the warmest 28 June 2019. It was shown that differences among two way precipitation forecasts are higher for longer forecasting periods than shorter ones, while in the case of 10m wind forecasts such dependence is not obvious. Further research is required for more precise quantification of forecasts comparison with and without assimilation of upper air wind for Dubrovnik weather station.

References

Daley, R. 1991: *Atmospheric data analysis.* Cambridge university press, Cambridge. 457 pp.

Hollingsworth A.,Lönnberg P.1986: The statistical structure of short range forecast errors as determined from radiosonde data . Part I: The wind field. *Tellus 38 A*: 111-136.

Ivančan Picek B., Horvath K., Strelec Mahović N., Gajić Čapka M. 2014: Forcing mechanisms of a heavy precipitation event in the southeastern Adriatic area. Nat Hazards, 72, 1231-1252.

Pandžić K. 2002: *Analysis of meteorological fields and systems* (in Croatian). HINUS, Zagreb. 314.

Pandžić K. and Likso T. 2005: Eastern Adriatic typical wind field patterns and large-scale atmospheric conditions. Int. J. Climatol. 25, 81-89.

Skamarock W.C., Klemp J.B., Dudhia J., Gill D.O., Barker D.M., Duda M.G., Huang X.Y., Wang W. and J.P. Powers J.P. 2008: Description of the advanced research WRF version 4, Rep. NCAR/TN-475+STR, National Center for Atmosphere Research, Boulder.